Engineering Science and Technology, an International Journal 19 (2016) 292–312

HOSTED BY

Contents lists available at ScienceDirect

Engineering Science and Technology, an International Journal

journal homepage: http://www.elsevier.com/locate/jestch

Full Length Article

Multi-objective optimization of steel nitriding

P. Cavaliere *, A. Perrone, A. Silvello

Department of Innovation Engineering, University of Salento, Via per Arnesano, Lecce I-73100, Italy

ARTICLE INFO

Article history:
Received 23 February 2015
Received in revised form
24 June 2015
Accepted 13 July 2015
Available online 8 September 2015

Keywords:
Nitriding
Mechanical properties
Optimization

ABSTRACT

Steel nitriding is a thermo-chemical process largely employed in the machine components production to solve mainly wear and fatigue damage in materials. The process is strongly influenced by many different variables such as steel composition, nitrogen potential (range 0.8–35), temperature (range 350–1200 °C), time (range 2–180 hours). In the present study, the influence of such parameters affecting the nitriding layers' thickness, hardness, composition and residual stress was evaluated. The aim was to streamline the process by numerical–experimental analysis allowing to define the optimal conditions for the success of the process. The optimization software that was used is modeFRONTIER (Esteco), through which was defined a set of input parameters (steel composition, nitrogen potential, nitriding time, etc.) evaluated on the basis of an optimization algorithm carefully chosen for the multi-objective analysis. The mechanical and microstructural results belonging to the nitriding process, performed with different processing conditions for various steels, are presented. The data were employed to obtain the analytical equations describing nitriding behavior as a function of nitriding parameters and steel composition. The obtained model was validated through control designs and optimized by taking into account physical and processing conditions.

1. Introduction

The deep analysis of industrial processes depending on different parameters necessitates the employment of computational multi objective optimization tools. Optimization is the key to reach this goal, achievable through integration with multiple calculation tools and explicable by effective post-processing tools. modeFRONTIER platform allows the organization of a wide range of software and an easy management of the entire product development process. The role of the optimization algorithm is to identify the solutions which lie on the trade-off curve, known as the Pareto Frontier. These solutions all have the characteristic that none of the objectives can be improved without prejudicing another. The time to run a single analysis makes running more than a few simulations prohibitive and some other smart approaches are needed. These factors lead to a Design of Experiment (DoE) technique to perform a reduced number of calculations. After that, these well-distributed results can be used to create an interpolating surface. This surface represents a meta-model of the original problem and can be used to perform the optimization without computing any further analyses.

Once data have been obtained, whether from an optimization or DoE, or from data importation, the user can turn to the extensive post-processing features in modeFRONTIER to analyze the results.

Not so many papers are available in literature on the analysis on thermo-mechanical diffusion processes of nitriding based on the Fick's laws model. In the present paper we are going to describe the behavior of nitriding process on different steels (40 different materials) in a broad range of processing parameters (600 experimental conditions) leading to the description of the effect on the steel structures and the subsequent mechanical properties. In Reference 1 the authors give a mathematical description to predict the nitrogen contents as well as residual stresses and distortions after nitride quenching. The model was implemented in finite element calculations in order to identify the profiles. They concluded that the interactions between diffusion of nitrogen also need to be established. As a general point of view, in fact, the hardening of steels during the nitriding process is due to the N-based compounds precipitation [2]. In such a way the precipitation sequence is strongly influenced by the compounds time formation of the single elements that must be largely considered in such kind of analysis. Several nitrogen mass transfer mechanisms have been proposed concerning the generation of nitriding species and interactions between ions, neutrals and steel surfaces. In Reference 3, the authors analyzed the nitriding process by employing the Mullins–Sekerka analysis on the interface separating a growing nitride layer in pure

* Corresponding author. Tel.: +39 0832297357, fax: +39 0832325004.
E-mail address: pasquale.cavaliere@unisalento.it (P. Cavaliere).
Peer review under responsibility of Karabuk University.

http://dx.doi.org/10.1016/j.jestch.2015.07.004

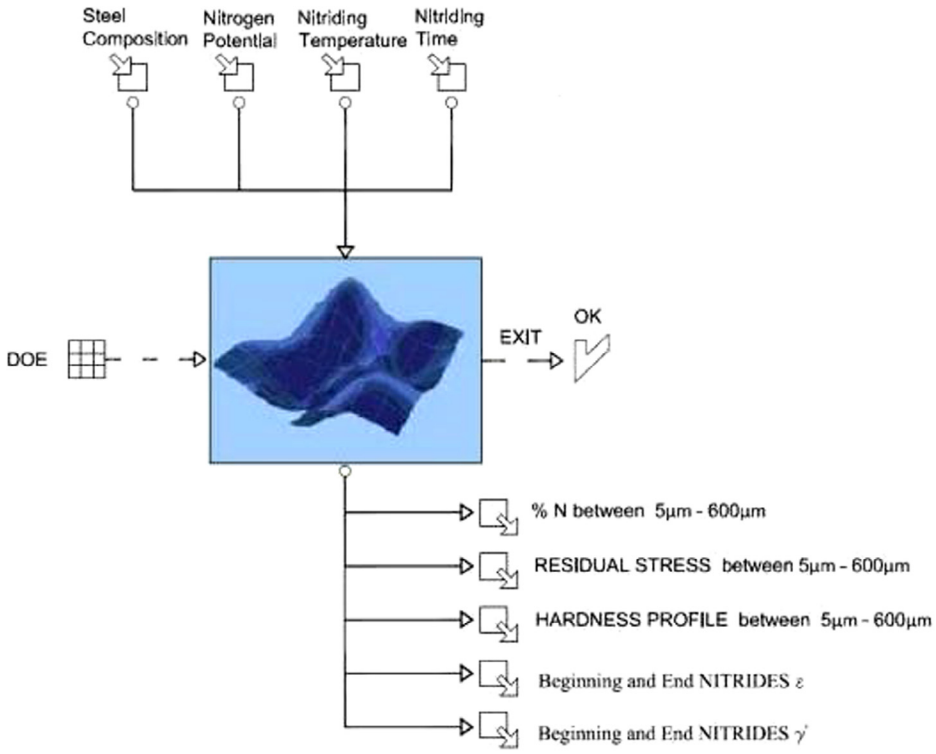

Fig. 1. Workflow of analysis.

iron. They showed that a plane interface is unconditionally stable due to the favorable combination of the Gibbs–Thomson effect and of the concentration fields. This result is specific to the nitriding configuration where the net flux of nitrogen necessary for the growth of the layer is in the growth direction. The influence of compositional and misfit generated stresses on the morphological stability has been discussed qualitatively. For these reasons, in the present paper, a large attention was devoted to the measurement and the control of compound layers and their effect on mechanical properties.

Other authors described results of simulations of the diffusional process of nitrogen on pure iron by putting emphasis on choice of the nitriding potential of NH_3–H_2 atmosphere on microstructural constitution and growth kinetics of nitride layers. On the basis of latest investigations about experimental results from nitrogen absorption-isotherms theory, they have shown that it is possible to predict both microstructural nature and thickness of nitrided layers as well as the nitrogen profile within the formed phases during gas nitriding [4,5]. In Reference 6, a generalized Wagner diffusion model

Table 1
Composition of some of the steels analyzed in the present study.

Steel	C	Si	Cu	Mn	Cr	Ni	Mo	Al	Ti	V	Nb	S	Co	W	N	P
	%	%	%	%	%	%	%	%	%	%	%	%	%	%	%	%
AISI1020	0.2	0.8	0	0.9	13	0	0	0	0	0	0	0.02	0	0	0	0.01
15CrMoV5-9	0.05	0.6	0.8	1.1	18.3	8.5	0	0	0.01	0	0	0.01	0	0	0	0.01
AISI5115	0.16	0.28	0	1.15	0.95	0	0	0	0	0	0	0.01	0	0	0	0.01
25CrMo20	0.25	0	0	0	5	0	0.2	0	0	0	0	0.01	0	0	0	0.015
31CrMo12	0.3	0.3	0	0.7	3.2	0	0.35	0	0	0	0	0.01	0	0	0	0.01
32CrMoV13	0.28	0.35	0	1.54	0.26	0	0	0	0	0.11	0	0.012	0	0	0	0.015
34CrNiMo6	0.38	0.26	0	0.7	0.8	0.7	0.22	0	0	0	0	0.01	0	0	0	0.02
34CrAlNi7	0.34	0	0	0	1.7	1	0.2	1	0	0	0	0.01	0	0	0	0.01
39NiCrMo3	0.4	0.3	0	0.7	1	1	0.2	0	0	0	0	0.02	0	0	0	0.01
42CrMo4	0.38	0.4	0	0.65	1.2	0	0.15	0	0	0	0	0.015	0	0	0	0.015
50VCr11	0.45	0.5	0	1	11	0.7	0	0	0	0.3	0	0.03	0	0	0	0.03
AISI304	0.05	0.56	0.8	1.12	18.3	8.5	0	0	0.01	0	0	0.012	0	0	0	0.013
AISI316L	0.07	1.00	0	2.00	17.50	12.00	2.00	0	0	0	0	0.03	0	0	0	0.05
X6Cr17	0.08	0	1	1	17	0	0	0.3	0	0	0	0.015	0	0	0	0.04
AISI410	0.12	1	0	1.5	13	0.75	0	0	0	0	0	0.015	0	0	0	0.04
AISI431	0.2	0.8	0	0.8	16	2	0	0	0	0	0	0.02	0	0	0	0.015
AISI4140	0.4	0.5	0	1.1	1	0	0.2	0	0	0	0	0.04	0	0	0	0.035
AISI4340	0.4	0.25	0	0.7	0.8	1.85	0.25	0	0	0	0	0.02	0	0	0	0.015
AISI7140	0.42	0.3	0	0.55	1.6	0	0.38	1	0	0	0	0	0	0	0	0
H10	0.36	0.39	0	0.32	2.96	0	2.86	0	0	0.41	0	0.002	0	0	0	0.03
H11	0.42	1.22	0	0.49	5.1	0	1.27	0	0	0.44	0	0	0	0	0	0
H12	0.36	0.87	0	0.43	5	0	1.7	0	0	0.33	0	0.01	0	1.15	0	0.01
H13	0.37	1	0	0.45	5.33	0.08	1.24	0	0	0.83	0	0.015	0	0	0	0.01

Table 2
Example of nitriding input parameters employed in the present study.

Steel	T_H	N_p	T_N	t_N
	°C	%	°C	h
AISI1020	550	12	350	0.5
15CrMoV5-9	433	26	430	179
AISI5115	170	6	510	50
25CrMo20	600	3	520	1
31CrMo12	570	3	520	30
32CrMoV13	600	1.5	550	100
34CrNiMo6	571	14.4	510	176
34CrAlNi7	600	1.2	500	3
39NiCrMo3	552	5.6	1180	40
42CrMo4	600	1.3	550	6.5
50VCr11	420	3	520	1
AISI304	20	10	580	5.5
AISI316L	20	35	500	5
X6Cr17	600	15	450	24
AISI410	720	3	520	20
AISI431	799	20.8	925	128
AISI4140	560	6	550	14
AISI4340	588	11.4	1185	143
AISI7140	570	12.4	930	124.5
H10	600	15	510	12
H11	486	21	1200	150.5
H12	600	15	580	8
H13	540	17.4	750	33.5

was used to analyze the layer formation and growth in definite experiments on plasma nitriding of pure iron. It was demonstrated that the model is able to predict the compound layer composition and can be used as a method for calculation of the effective diffusion coefficients in the first sublayer of the compound zone, providing that the concentration ranges and the effective diffusion coefficients of the nitrogen in the other sub-layers, as well as the total compound layer thickness as a function of time, are known. The thickness of the compound layer and the diffusion zone as well as their phase composition and the consequent mechanical properties depend on the nitriding temperature and time, which, in turn, depend on the nitrogen activity of the medium in which the nitriding process is taking place. In addition such chemical–physical processes depend on the state of the material before nitriding [7]. For this reason, in the present multi-objective optimization analysis the state of the material (in particular the heat treatment temperature) before nitriding was taken into account. In Reference 8 the authors modeled the nitrogen decomposition on the steel surface as a consequence of processing parameters. In Reference 9 the authors evidence the nitride layers formation in high temperature gas nitriding of stainless steel. In References 10 and 11 other authors underline the nitriding properties of steel after treatment at high temperatures up to 1050 °C. In Reference 12 the authors model the process through finite element analyses by employing microstructural data obtained from X-ray diffraction measurements. The same methods for microstructural evolution monitoring is described in Reference 13. The method is largely described in References 14 and 15 with experimental evidence. In References 16–18 the authors analyze the microstructural evolution of nitride layers through X-ray diffraction and model the nitriding behavior of H13 tool steel through a finite method. In References 19 and 20 the authors modeled the nitriding behavior through the analyses of compound layer thickness. The aim of the present paper is the complete experimental-numerical analyses of a nitriding process useful in designing a platform capable of analyzing the best conditions to reach high performances of nitride components or designing specific steel capable of being nitride in order to reach specific performances under fixed processing conditions. The strength of the analyses is due to the large quantity of data employed to develop the proposed model.

2. Experimental procedure

Steel cylindrical samples 100 mm in diameter were nitrided by varying the nitrogen potential, nitriding temperature and time. Nitriding process was performed in a laboratory furnace equipped with a sensor capable of performing measurements of nitrogen potential in the furnace atmosphere, in this way it was possible to precisely control the ammonia flux in the furnace. The sensor is sensible to hydrogen concentration that varies with ammonia dissociation. In this way it is possible to control the ammonia flux in order to fix the nitrogen potential. Compositional measurements were performed through EDX microanalyses in a Zeiss EVO40 SEM. Residual stresses and nitride thickness layer measurements were

Table 3
Example of output results measured after nitriding.

Steel	N_0	N_200	εs	εf	γ's	γ'f	Hv_0	Hv_200	σ_0	σ_100
	%	%	μm	μm	μm	μm			MPa	MPa
AISI1020	0.2	0	0	2	0	2	340	290	–70	–65
15CrMoV5-9	3	0.1	0	20	0	130	870	520	–130	–310
AISI5115	3	0.4	0	60	0	210	750	600	–110	–310
25CrMo20	0.4	0	0	5	0	25	450	310	–50	–160
31CrMo12	3	0.2	0	25	0	160	950	800	–400	–600
32CrMoV13	1.4	1.4	0	30	0	210	870	720	–350	–450
34CrNiMo6	6	0.7	0	170	0	510	990	560	–140	–250
34CrAlNi7	1	0	0	5	0	70	850	400	–260	–280
39NiCrMo3	3	0	0	5	0	25	620	340	–140	–380
42CrMo4	1.3	0.3	0	25	0	360	700	500	–50	–70
50VCr11	1.3	0	0	40	0	45	1100	380	–80	–170
AISI304	10	0	0	32	0	75	1280	200	–200	–120
AISI316L	21	0	0	20	0	40	1100	1060	–280	–200
X6Cr17	9	0	0	30	0	45	1220	260	–90	–170
AISI410	2	0.2	0	65	0	180	1200	320	–400	–540
AISI431	1.2	0	0	6	0	21	590	230	–140	–460
AISI4140	4	0.6	0	80	0	320	750	520	–130	–160
AISI4340	7	0	0	7	0	14	470	210	–140	–390
AISI7140	2	0	0	15	0	90	640	210	–110	–170
H10	14	0.1	0	20	0	140	1100	510	–230	–420
H11	11	0	0	30	0	90	840	140	–180	–490
H12	8	0	0	18	0	170	1070	300	–200	–540
H13	11	0	0	2	0	11	970	280	–290	–620

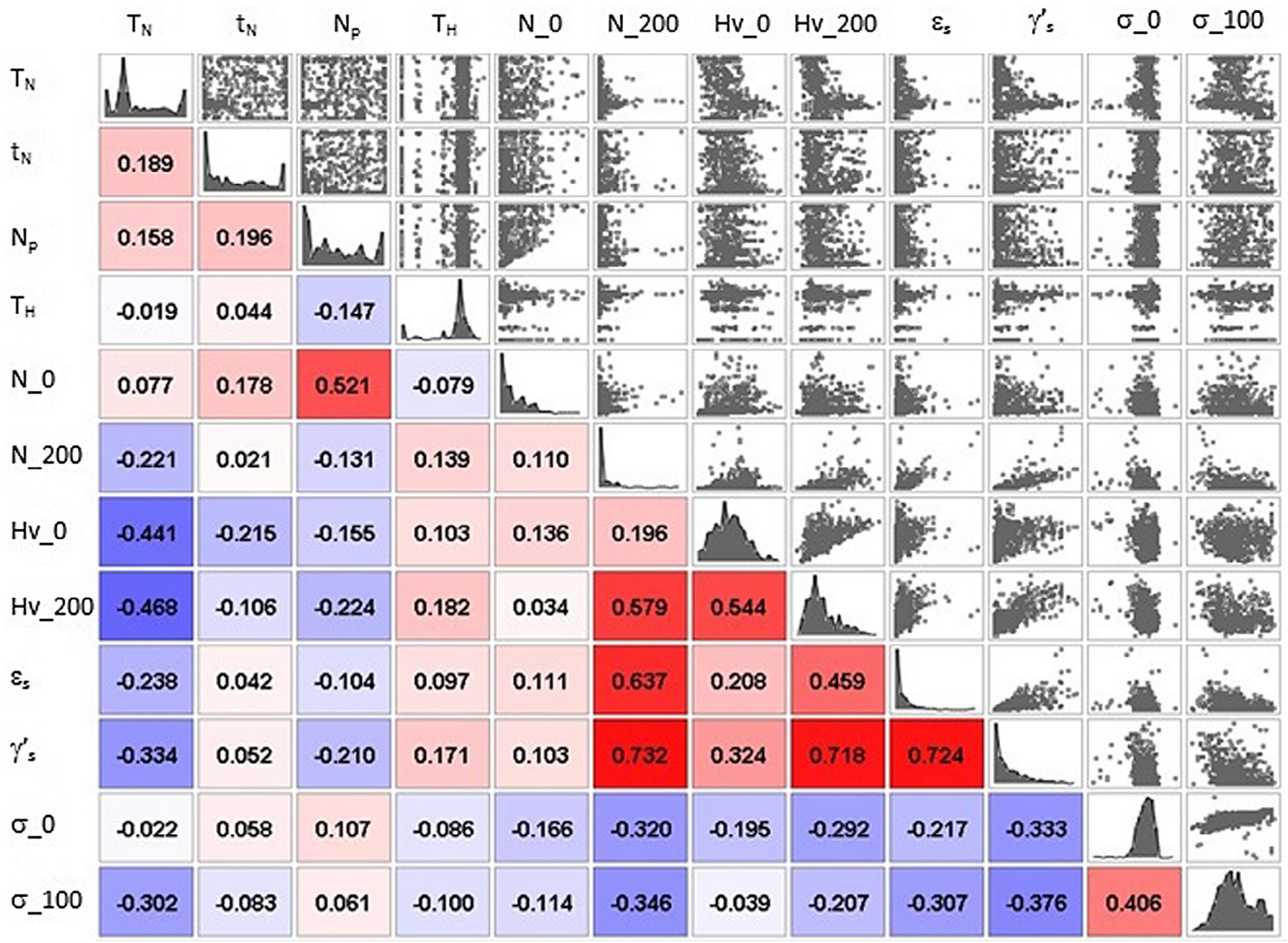

Fig. 2. Correlation matrix of the different inputs–outputs analyzed in the present study.

performed through X-ray diffraction by using a Rigaku Ultima+ diffractometer by employing Hall–Williamson plotting. The Hall–Williamson method [21] is based on the principle that the lattice size broadening and strain broadening vary quite differently with respect to Bragg angle. By scannning a surface with X-rays and measuring the peak shifts of the spectrum, residual strains (and residual stresses) can be measured. Samples were cut along the center section, ground and polished, then the residual stresses were measured from the surface to the bulk. Microhardness was measured by employing a Vickers indenter with a 1000 gf load for 15 s.

Starting from a database built with experimental results, computational models (virtual n-dimensional surfaces) able to reproduce at best during the actual process were developed. Through such analysis it was possible to optimize the output variables (% N, residual stress, beginning and end nidrides ε, beginning and end nidrides γ').

The method used for the creation of meta-models to simulate the actual process through the use of physical laws with appropriate coefficients to be calibrated was that of the RS.

This method consists of creating n-dimensional surfaces that are "trained" on the basis of actual input and output. These surfaces trained on a large experimental data can give the output numbers that reflect the real process of nitriding.

In the present study response surfaces (RS) that are best suited to deal with a multi-objective optimization were obtained. The available tools are the ones offered by modeFRONTIER, such as RS distance, the RS residual and RS function plot.

The experimental design consists of 600 input and output obtained from experimental data. To train the virtual surface in the training phase 580 experimental design inputs and outputs were included. The remaining 20 were used in the design validation phase.

The computational details were largely described by the authors in Reference 22.

The nitriding process through the analysis performed by modeFRONTIER is summarized in the workflow of Fig. 1.

The workflow is divided into the data flow (solid lines) and logic flow (dashed lines) having as their common node the computer node in which to introduce physical and mathematical functions representing the nitriding process. In the data flow all input parameters included are optimized in the numerical simulations:

- ✓ Steel composition
- ✓ Nitrogen potential
- ✓ Nitriding temperature
- ✓ Nitriding time

as well as the output parameters:

- ✓ % nitrogen hardened in the layer between 5 μm and 600 μm of distance from the surface of the sample

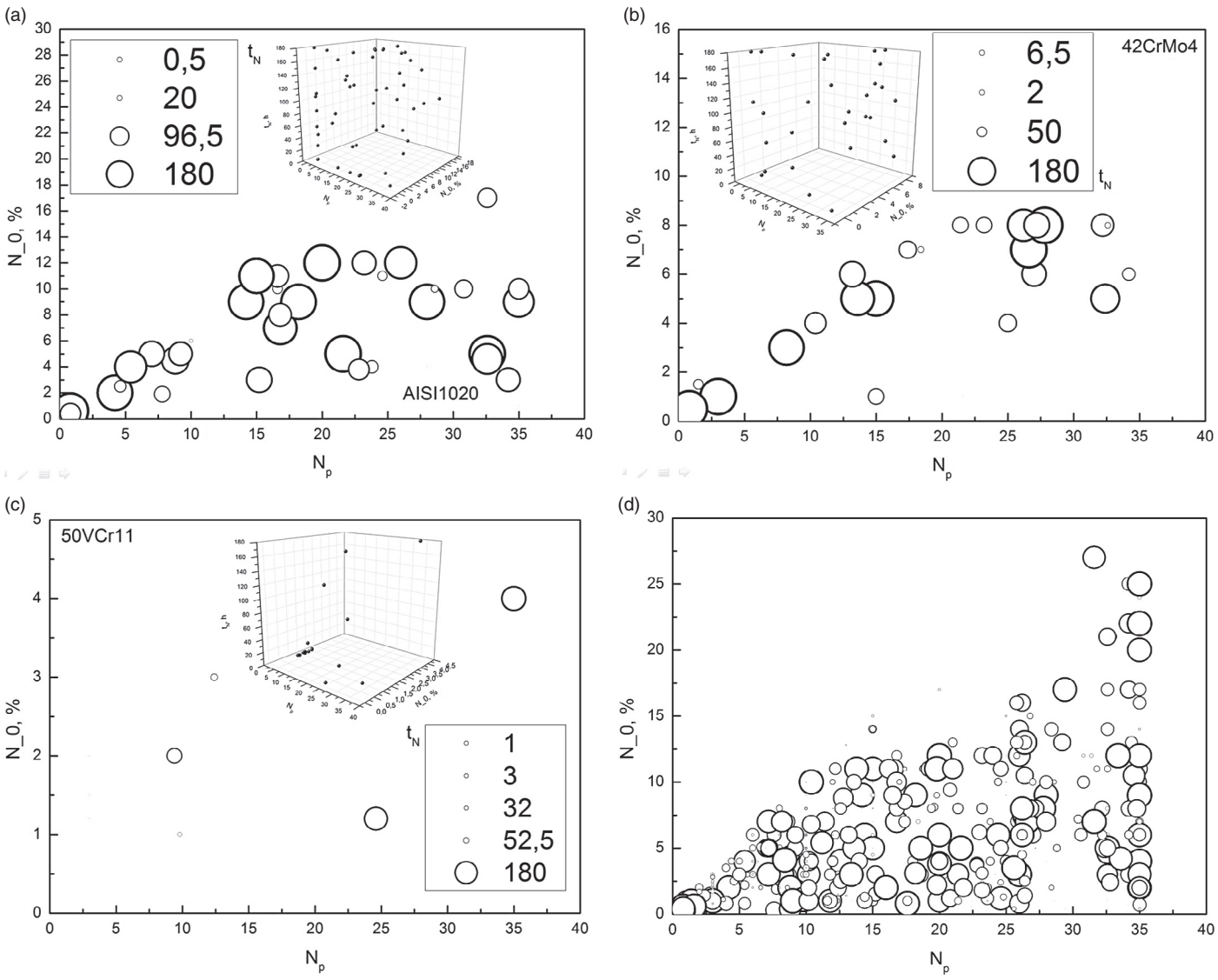

Fig. 3. Nitrogen concentration on the surface as a function of nitrogen potential and nitriding time for different steels and representative of all the collected data.

- ✓ Residual stress between 5 μm and 600 μm of distance from the surface of the sample
- ✓ Hardeness stress profile between 5 μm and 600 μm of distance from the surface of the sample
- ✓ Beginning and end nidrides ε
- ✓ Beginning and end nidrides γ'

The output variables define a multi goal analysis and have been minimized, taking into account some constraints or limitations typical of the actual process. At this stage the nodes that make up the logic flow of numerical analysis are defined. The first node is the DoE, which is the set of different designs reproducing different possible working conditions, among which the most affective ones are highlighted. Therefore it means creating a set number of designs that will be used by the scheduler (the node where the best algorithm is introduced) for the optimization. Depending on how this space is filled, the designs, defined by the scheduler, are more or less truthful. Therefore the choice of the DoE is to be assessed correctly.

Generally, in this kind of analysis, the heart of the optimization is represented by a series of equations of chemical and physical nature of a given resolution to get the desired output. In the present case, all this information is not clear, due to the complexity of the process and so it was chosen to employ the methodology of response surfaces. Optimization software allows the following of different kinds of RS. For each output variable to be minimized it is necessary to create a response surface. The analysis starts from a database built with data of operating conditions of the sintering plants obtained from experimental measurements and other related values found in the literature.

The database is divided into two main parts. The first one contains all the input parameters; the second one contains the corresponding output for each input conditions set.

The steel compositions and the nitriding input parameter examples, performed on the cyclindrical samples, are summarized in Tables 1 and 2.

3. Results and discussion

The output results corresponding to the steel compositions and input parameters previously shown are listed in Table 3. As a general behavior microhardness in steels is strongly dependent on nitriding temperature; on the contrary they are differently dependent on the nitrogen potential as a function of steel composition and nitriding time.

Of the 600 starting designs, 580 were used to generate metamodels, while 20 designs were employed as designs of control to verify the affordability of the response surfaces. These 20 were chosen in order to get the right information on the entire range of existence of the output variables.

The next step is to evaluate the performance surface and use them as a node operator in our work flow. Initially the tool RS distance, allowing to assess graphically the distance between the real values provided by the database and those generated by the virtual metamodel, was employed. The virtual profile is very close to that of the actual design.

It is important, in the present analysis, to employ the so called "correlation matrix" that allows to immediately recognize how much the different variables are correlated between each other; the parameters are actually strongly correlated if the corresponding value in the table is distant from zero in a range between –1 and 1, if the value is 1 the parameters are directly correlated, while if the value is –1 the parameters are inversely correlated. An example for the present study is given in Fig. 2, from such matrix it is also possible to observe the different weight of all the parameters, the more the value differs from 0 the more it influences the corresponding variable.

In the correlation matrix of Fig. 2, the nitrogen concentration, material hardness and residual stresses at different distances from the surface (0 and 200 μm for nitrogen and hardness, 0 and 100 μm for residual stresses) are shown; the ε and γ′ nitrides thickness layer dependences on nitriding parameters are also shown. In the case of nitriding hardening, the nitrogen concentration on the surface (N_0) is strongly dependent on nitrogen potential and on nitriding time, an example of bubble graph for AISI1020, 42CrMo4, 50VCr11 and all the collected data is given in Fig. 3.

Fig. 3a shows that nitrogen concentration on the samples surface increases with nitrogen potential and temperature increase for AISI1020. An example of linear increase is shown for 42CrMo4 steel (Fig. 3b). A non linear dependence is observed for other steels such as 50 CrV11 (Fig. 3c). The nitrogen concentration at 0.2 mm from the surface (N_200) is directly dependent on heat treating temperature before nitriding and inversely proportional to nitriding temperature and nitriding potential. The surface hardness (Hv_0) is dependent strongly on nitriding temperature, then on nitriding time (Fig. 4). A linear dependence on nitriding temperature and time is underlined for AISI1020 (Fig. 4a), for 42CrMo4 (Fig. 4b) and for 50CrV11 (Fig. 4c).

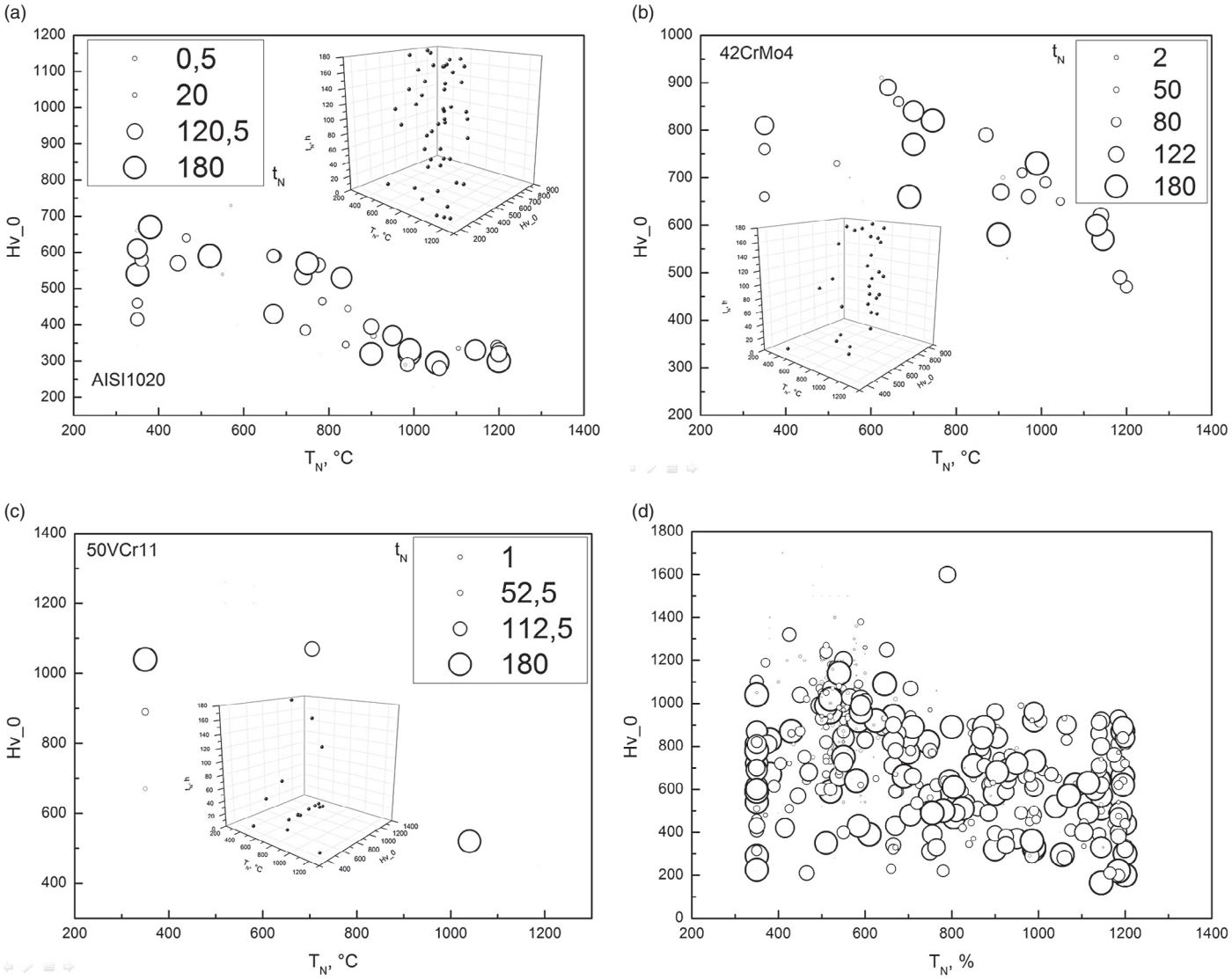

Fig. 4. Microhardness on the surface as a function of nitriding temperature and nitriding time for different steels and representative of all the collected data.

The microhardness at 0.2 mm from the surface (H_200) is dependent on the same parameters with almost the same weight. The residual stresses on the surface (σ_0) are dependent on the nitrogen potential while the residual stresses at 0.1 mm from the surface (hw_100) are dependent on nitriding temperature and heat treating temperature; the residual stresses are strongly the function of the compound layers formed during diffusion.

3.1. Analytical model

The nitriding process leads to steel hardening, thanks to the diffusion of nitrogen in the interstitial sites of iron leading to the precipitation of high hardness nitrides. Nitride layers are generally:

–Surface zone (5–30 μm) with varying portions of Feγ' Fe_4N (face centered cubic ductile phase) and $Fe_{2-3}N$ (HCP) more brittle but with very good wear properties.

–Another zone (0.05–0.8 mm) that results into a solid solution of nitrogen in the ferrite with the presence of nitrides in the form of very fine reinforcing particles (Fig. 5).

The analytical model relative to the equations employed to solve the Fick's laws to be implemented in the finite element code is largely described in Reference 2.

In the present approach, the evaluation of the dependence on the main input parameters on the nitrogen diffusion has been analyzed. The scatter matrix of the nitrogen diffusion as a function of input parameters is shown in Fig. 6.

In the surface layers a linear dependence on nitrogen potential can be underlined. The dependence tends to zero after 300 μm. In the inner layers a linear inverse proportionality with the nitriding temperature can be observed. In order to correlate the local nitrogen diffusion to the nitriding parameters it is useful to employ scatter charts relative to single points. In Fig. 7 the

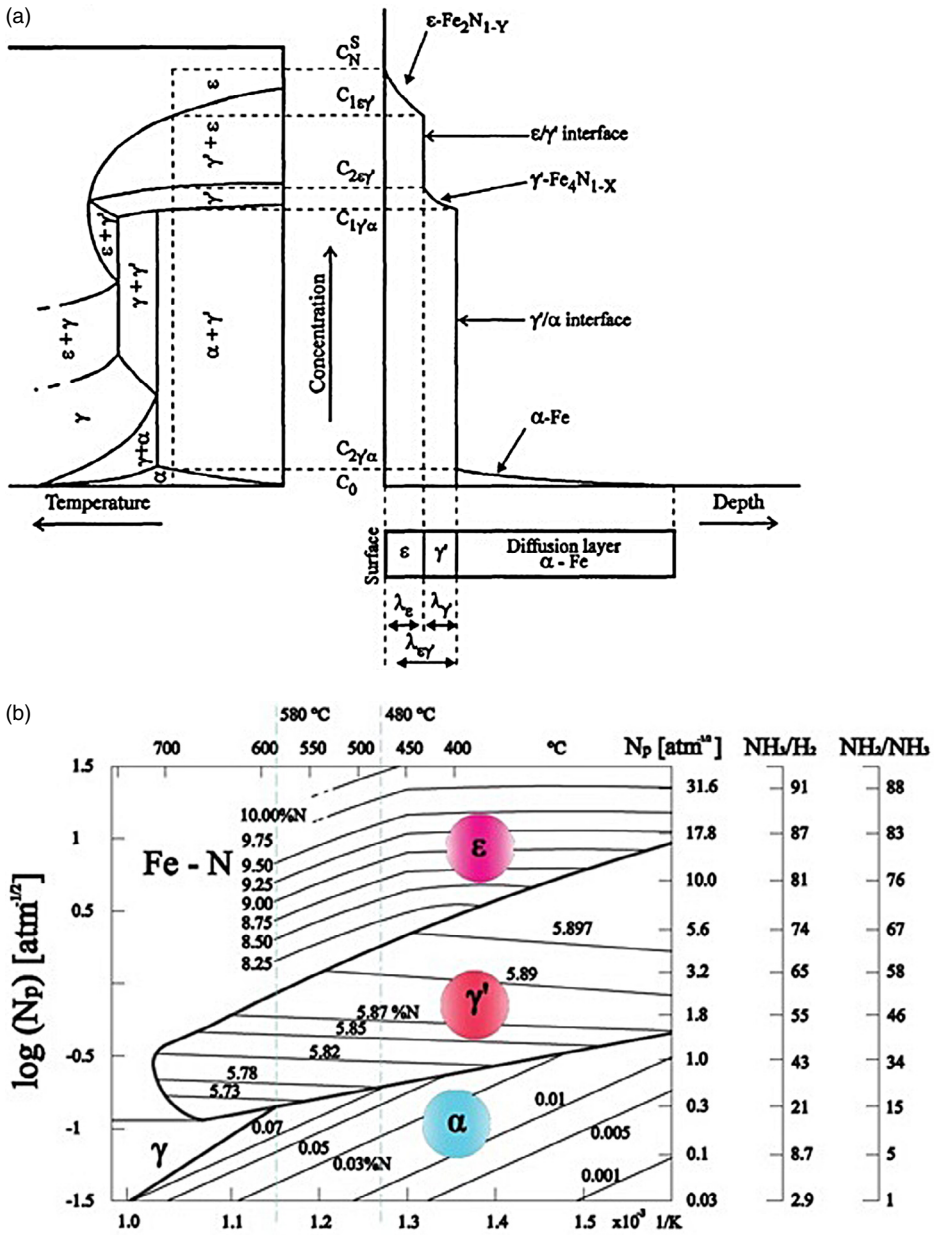

Fig. 5. Different hardening phases as a function of temperature and percentage of different elements in the Fe–N diagram (a); Leher diagram (b) Reference 1.

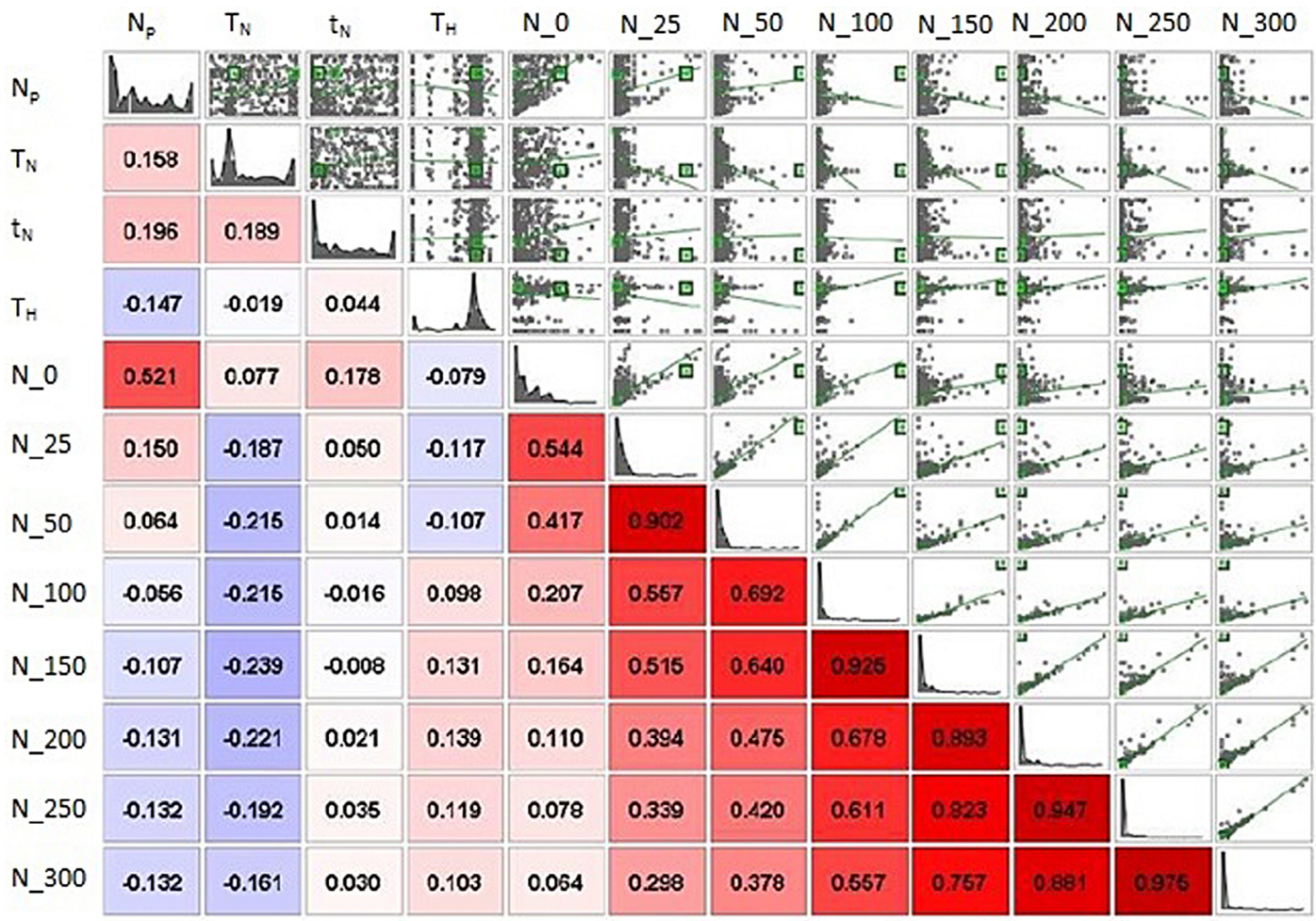

Fig. 6. Nitrogen concentration dependence on nitriding input parameters.

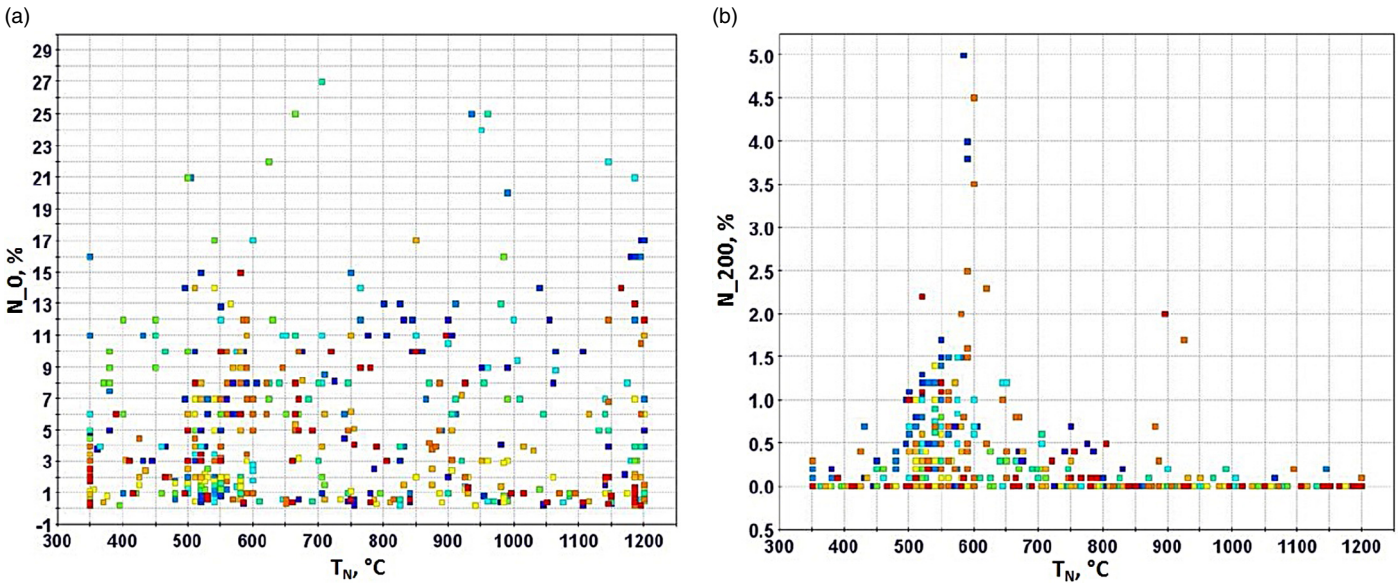

Fig. 7. Scatter charts describing the nitrogen concentration as a function of nitriding temperature on the surface and at 200 μm thickness.

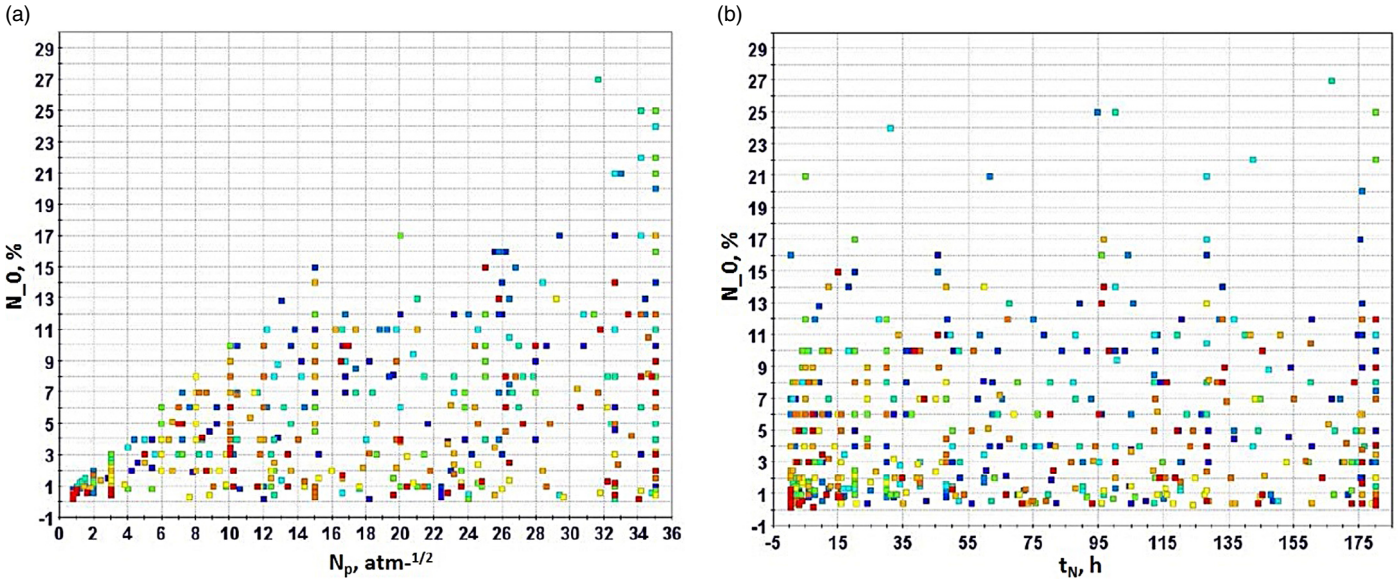

Fig. 8. Nitrogen concentration on the surface as a function of nitrogen potential and nitriding time.

nitrogen concentrations on the surface and at a thickness of 200 μm are described.

The optimal nitriding temperature for the maximum concentration of nitrogen on the surface is around 700 °C; the optimal nitriding temperature for the maximum concentration at 200 μm from the surface is 600 °C.

The nitrogen concentration on the surface is linearly dependent on the nitrogen potential while it seems less dependent on the nitriding time (Fig. 8). The different colored points refer to different processing conditions and steels.

With regards to the hardening phases formation the thickness of the different phases was monitored. The corresponding scatter matrix dependence is shown in Fig. 9.

The thickness of the hardening phases is non-linear dependent (in particular with regard to the nitriding temperature) on the input parameters. A local approach better describes these conditions. The singular hardening phases in nitriding are often overlapped. (CrN, AlN, TiN, . . .); in the present paper thicknesses of the different layers were evaluated through the coupled variation in hardness and residual stresses. The thickness of ε and γ′ as a function of nitriding temperature is shown in Fig. 10.

ε and γ′ reach their maximum thickness for a nitriding temperature around 600 °C. Their thickness increases as the nitrogen potential increases up to 10 $atm^{-1/2}$, then a decrease is observed. Hardening phase thickness shows a maximum for a nitriding time around 15–20 h (Fig. 11).

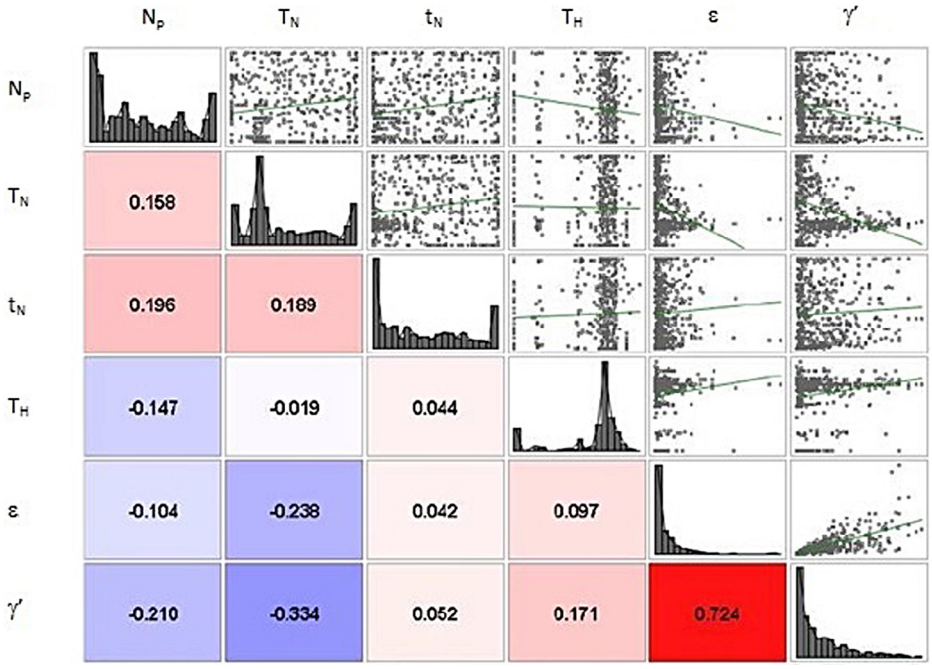

Fig. 9. Hardening phase thickness dependence on the nitriding input parameters.

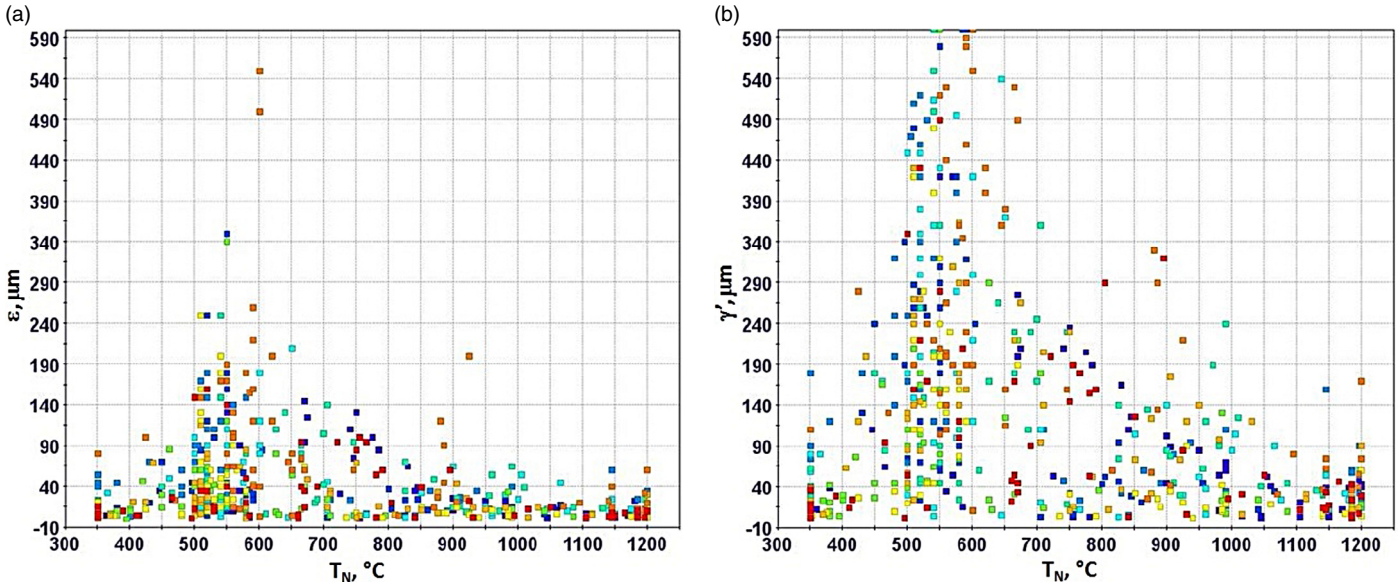

Fig. 10. Hardening phase thickness as a function of the nitriding temperature.

The experimental results of the present study demonstrated that the nitrogen potential influences the maximum hardness values on the surface. On the contrary, the nitrogen potential does not influence the hardness profile, it is strongly influenced by the steel composition. The corresponding scatter matrix shows the correlation between the nitriding parameters and the hardness profile (Fig. 12).

It is difficult, in such a case, to give some linear dependence of the hardness profile on the nitriding processing conditions. By taking into account a local approach we can observe that the surface hardness increases with increasing nitrogen potential for low values, then it decreases with increasing nitrogen potential (Fig. 13a). The surface hardness linearly increases as the nitriding temperature increases up to 500–550 °C, then the surface hardness decreases as the nitriding temperature increases (Fig. 13b).

An inverse dependence of hardness with nitriding time was observed. A very interesting phenomena is the relationship between the hardness of the inner layers and the γ' phase behavior, in particular, a linear increase in the inner hardness is related to an increase in the γ' phase (Fig. 14).

Residual stresses in nitride components are mainly due to the nitrides expansion into the ferrite matrix. Residual stresses are mainly governed by the nitriding temperature with a strong drop for temperatures in the range 550–600 °C (Fig. 15).

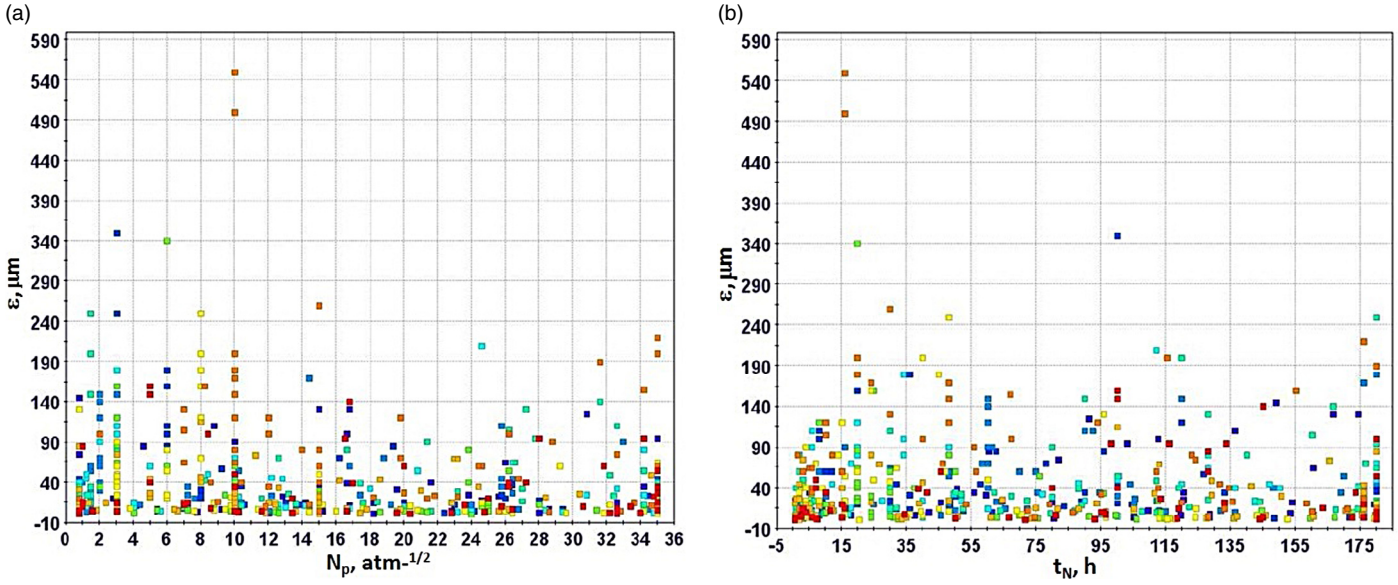

Fig. 11. ε phase thickness as a function of nitriding temperature and time.

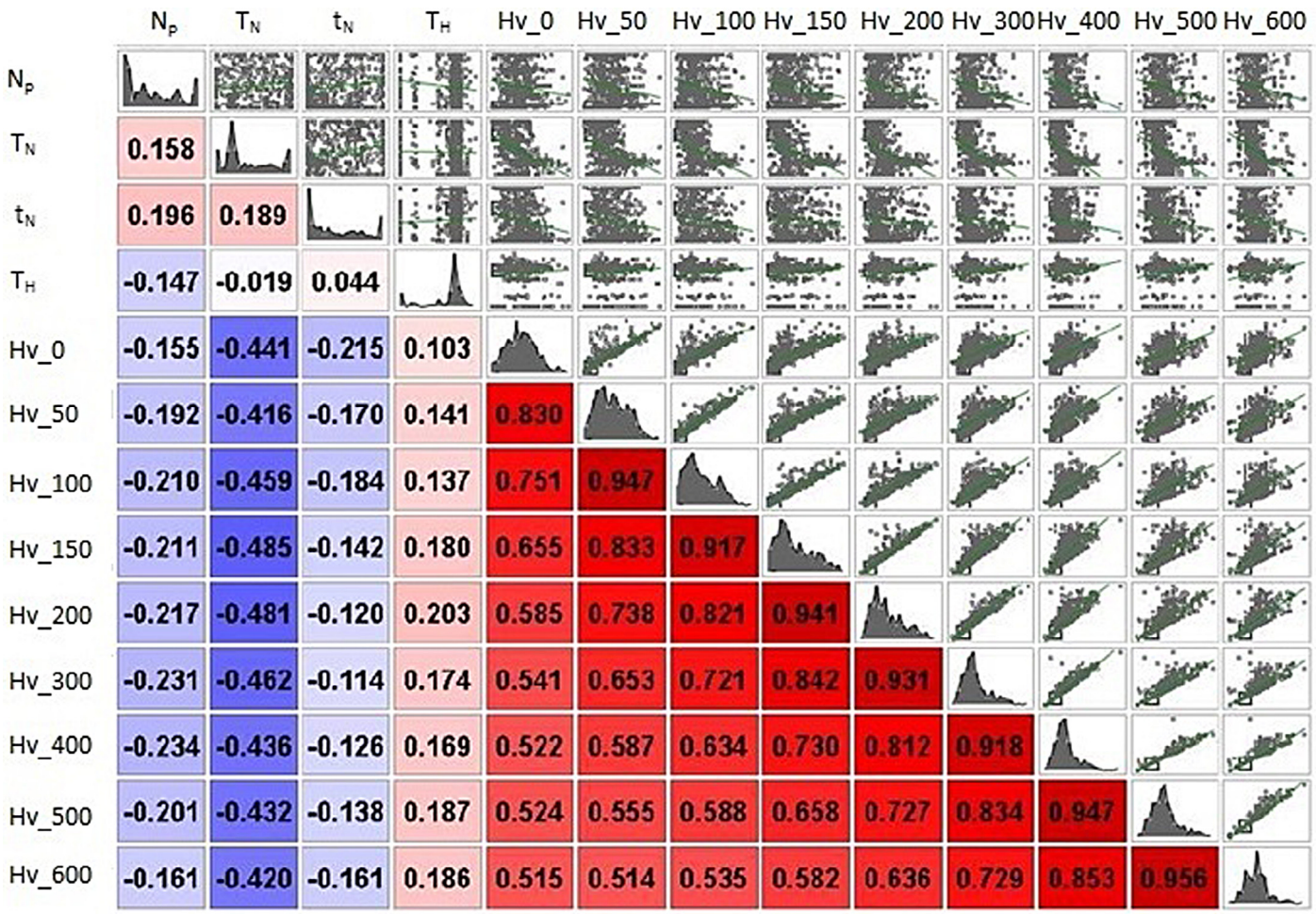

Fig. 12. Hardness dependence on the nitriding processing conditions.

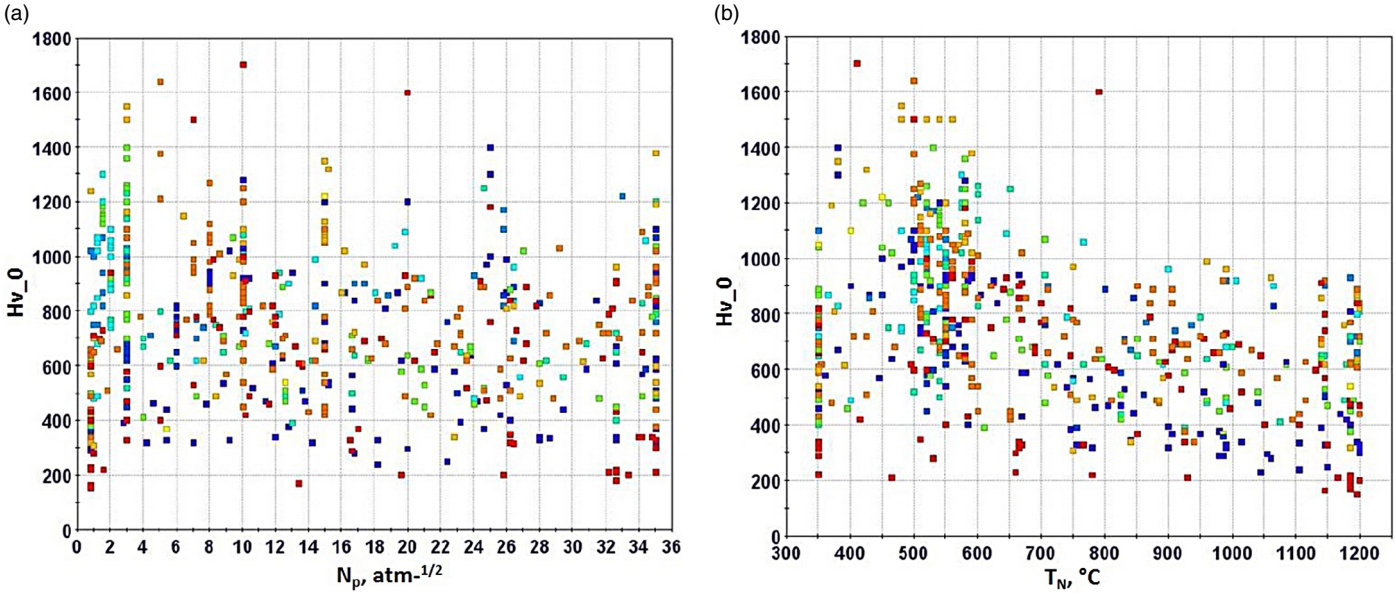

Fig. 13. Surface hardness dependence on nitrogen potential (a) and on nitriding temperature (b).

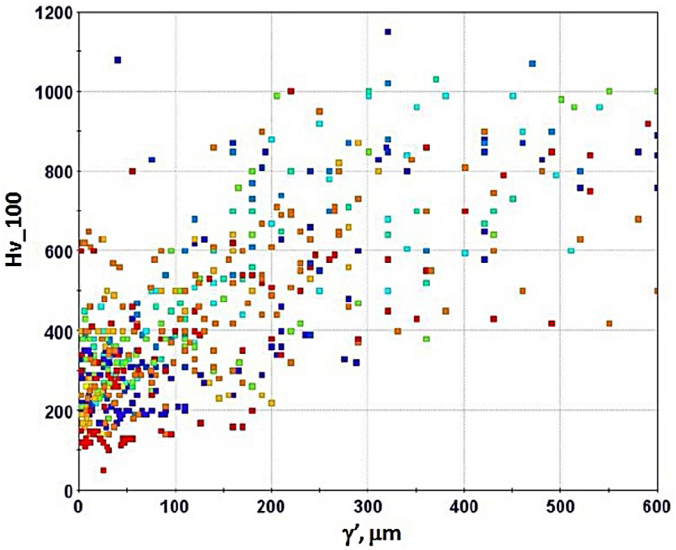

Fig. 14. Hardness dependence on γ' phase thickness.

All the results provided by modeFRONTIER can be employed to develop an analytical instrument to predict the diffusional and mechanical properties of nitrided specimens. The main result of this phase is the possibility to obtain the dependence of microstructural and mechanical properties of the nitrided materials as a function of all the employed input parameters. An example of such equations (Eqs. A1–A5), describing the dependences of carbon concentration, martensite phase, hardness and residual stresses at a thickness of 0.05 mm, is reported in the Appendix.

3.2. Validation

The input parameters training set is underlined in Tables 4 and 5.

The validation set obtained by modeFRONTIER computation is described in Fig. 16.

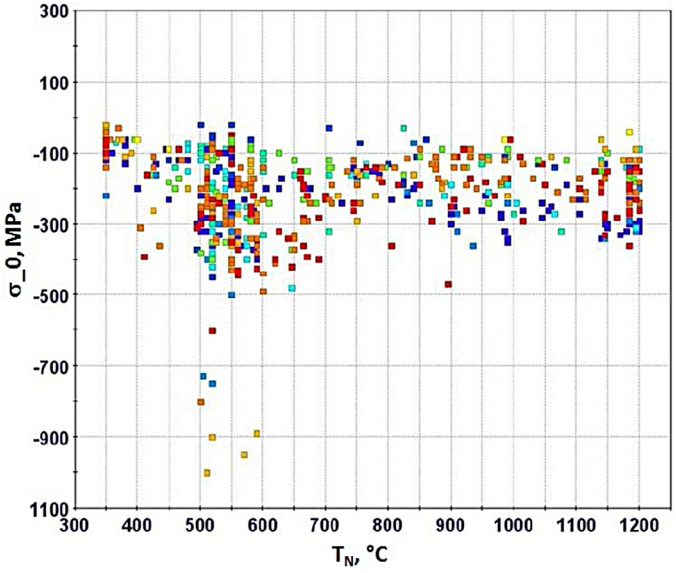

Fig. 15. Surface residual stresses dependence on nitriding temperature.

Table 4
Compositional limits of the nitride steels.

Element (%)	Fe	C	Si	Cu	Mn	Cr	Ni	Mo	Al	Ti	V	Co	W
Min.	63.9	0.01	0	0	0	0	0	0	0	0	0	0	0
Max.	100	2.4	1.22	3	2.24	20	12	4.75	1.1	0.5	9.8	12.1	6

For the selected conditions the experimental and numerical results were compared.

The results in terms of microhardness, nitrogen profile and residual stresses of the control designs are shown in Figs. 17–20. The nitriding conditions are described in Table 6.

In all the validation designs an excellent agreement between experimental and numerical results for the nitrogen and microhardness profiles can be recorded. In some cases such agreement differs for the residual stress profiles probably depending on the range of experimental input fixed for the singular steel (e.g. AISI 304).

For the main validation designs the calculation of the precipitation layers' thickness is also in good agreement with the experimental measurements (Fig. 21). The nitriding conditions for each control design are described in Table 6.

The Mean Square Error (MSE) applied on the points of measurement of the specific size of output was employed for the error calculation. Expressing the discrepancy between experimental and numerical values as follows:

$$\Delta y_i = y_{\exp,i} - y_{num,i} \tag{1}$$

the Mean Square Error (MSE) for the outputs representative of a point is equal to:

$$MSE = \sum_{i=1}^{5} \frac{(\Delta y_i)^2}{5} \tag{2}$$

The mean square error for the 10 selected control designs is given in Table 7:

Table 5
Input parameter limits.

T_H (°C)	N_p (%)	T_N (°C)	t_n (h)
0	0.8	350	0.5
799	35	1200	180

Table 6
Nitriding conditions for the control designs.

Steel	T_H °C	N_p %	T_N °C	t_N h
AISI1020	595	8.8	740	136.5
15CrMoV5-9	500	8	550	50
31CrMo12	523	35	495	58
34CrAlNi7	550	26.4	900	128
39MoAlCr15	570	12.6	1175	87
AISI304	20.0	10	500	20
AISI420	640	3	540	4
M2	614	1.4	930	176
V2	618	28.8	885	56
18HGT	617	26.8	885	131.5

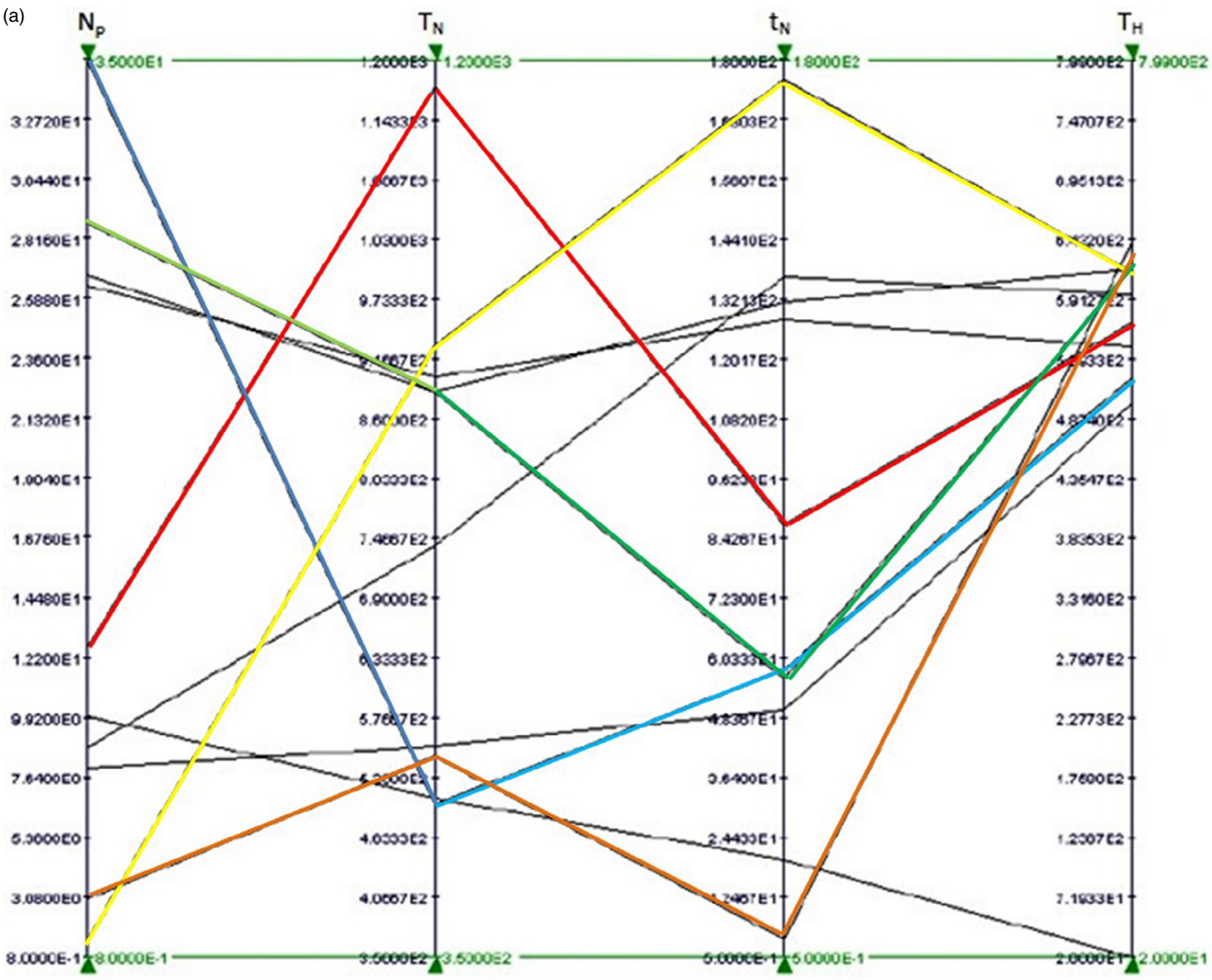

Fig. 16. Validation set of nitriding conditions.

Table 7
Mean square error for the nitriding output for each selected control design.

Design	N(%)	Hv (Vickers)	ε (μm)	γ′ (μm)	σ (MPa)
1	0.45	19.32	0.61	18.85	69.79
2	0.18	28.15	0.58	29.60	103.7
3	1.79	97.04	38.88	111.81	85.84
4	0.33	49.07	10.12	51.66	47.81
5	1.5	83.23	7.47	35.13	61.86
6	0.07	59.62	0.33	13.43	97.84
7	0.05	134.65	2.60	35.26	24.37
8	0.28	38.53	1.3	9.33	108.99
9	0.44	35.91	51.96	17.38	46.29
10	0.45	35.21	21.19	14.49	58.33

3.3. FEM (finite element modeling) calculation and optimization

The finite element calculations were performed on cylindrical samples. The mesh geometry was realized with much more elements on the sample surface (Fig. 22).

The material database is built by assigning the nitriding performances for each steel in terms of compositions, in this way it is possible to choose the optimal steel for each needed nitriding output and, at the end of the optimization phase, design a specific steel to reach the needed nitride conditions. In the first case it is possible to perform the simulation with fixed nitriding conditions on a different steel in order to choose the best composition fitting with the needed mechanical properties. The second case is realized for those conditions in which the user needs to design new steel for very specific performances. The platform is designed to fix up to 3 objective functions in terms of mechanical properties (hardness, nitrogen concentration, residual stresses). All the input parameters are given to the meta-models through modeFRONTIER. The post processing of the runs is the optimization phase.

In the optimization study different objective functions were identified to be related to mechanical properties to be optimized under physical constraints. The identified mechanical properties were hardness and residual stresses. By taking a look at the hardness behavior it was decided to maximize the bulk hardness at a different distance

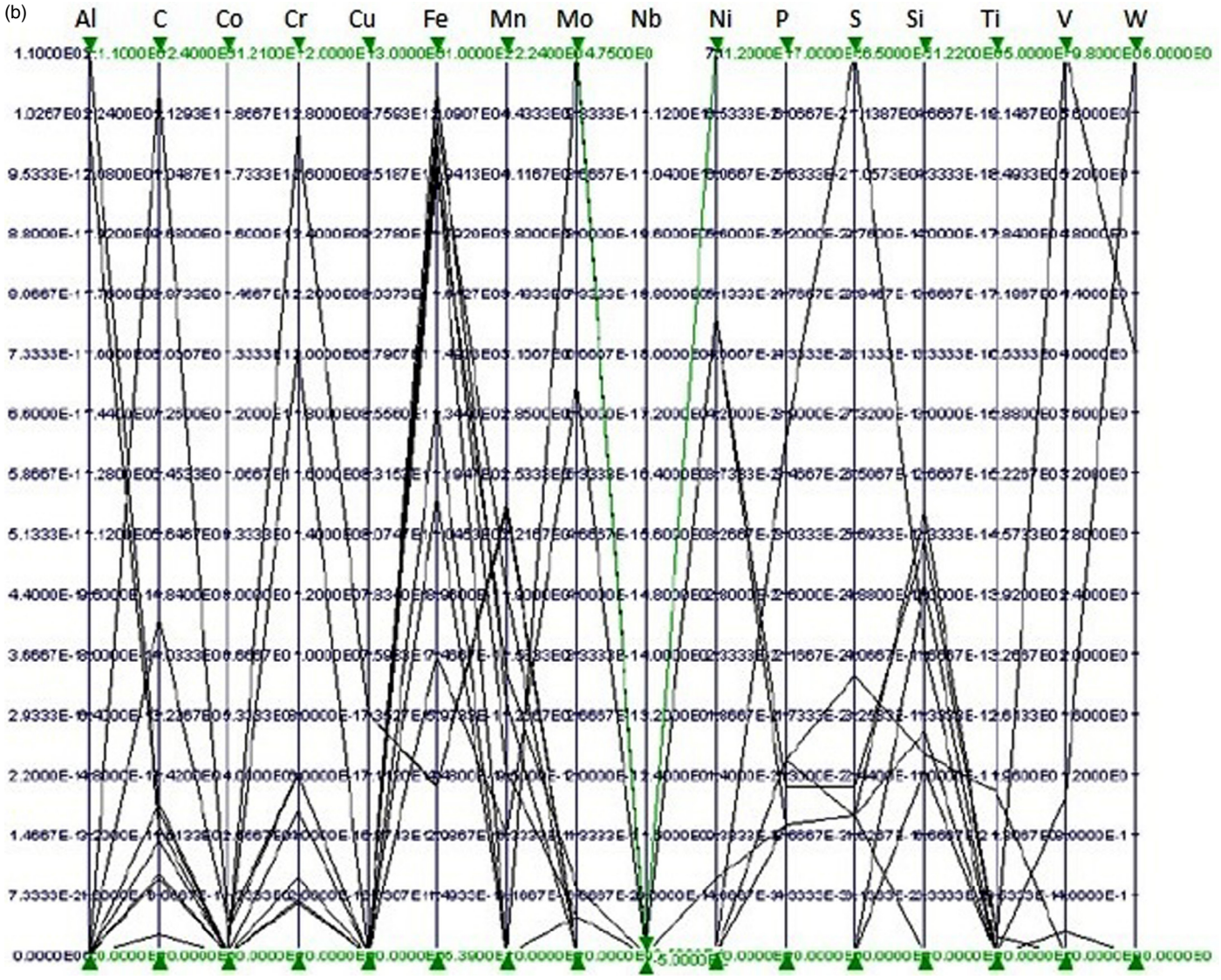

Fig. 16. (*continued*)

from the surface and the surface hardness. After the convergence test, the Pareto analyses allow to identify the better compromise between the two functions. The results showed an excellent agreement for the nitrogen concentration and hardness, a more pronounced shift of numerical data from experimental ones can be underlined for the residual stresses. At the end of the analyses the hardness profiles as a function of the number of runs were identified (Fig. 23), and for those profiles the processing parameters to be employed for the achievement of the desired mechanical properties were obtained (Fig. 24).

4. Conclusions

In the present paper experimental data, finite element calculations, and multi-objective optimization were integrated in order to develop a model capable of predicting mechanical properties, microstructural evolution and phase transformations during steel nitriding as a function of chemical compositions of steel and processing parameters. From the experimental results the mapping of nitrogen concentration, microhardness, residual stresses, precipitate distribution as a function of different processing parameters for various steels was obtained. The results were summarized in a database useful for further analyses, in particular to obtain the data to be compared with the numerical ones. From the analyses of the correlation matrices it was calculated that nitrogen concentration on the surface is strongly dependent on nitrogen potential and on nitriding time; surface hardness is dependent strongly on nitriding temperature; residual stresses on the surface are dependent on the nitrogen potential while the residual stresses in the inner layers are dependent on nitriding temperature; residual stresses are strongly function of the compound layers formed during diffusion. A deep local analysis allowed calculating the dependence of mechanical and microstructural behavior, at fixed distances from the surface, on all the employed experimental processing parameters. All the data were employed for the calculation and optimization through modeFRONTIER and ANSYS in order to develop an analytical instrument capable of predicting the microstructure and mechanical properties of steels during nitriding in a broad range of conditions. In particular, a generalized solution of the Fick's law

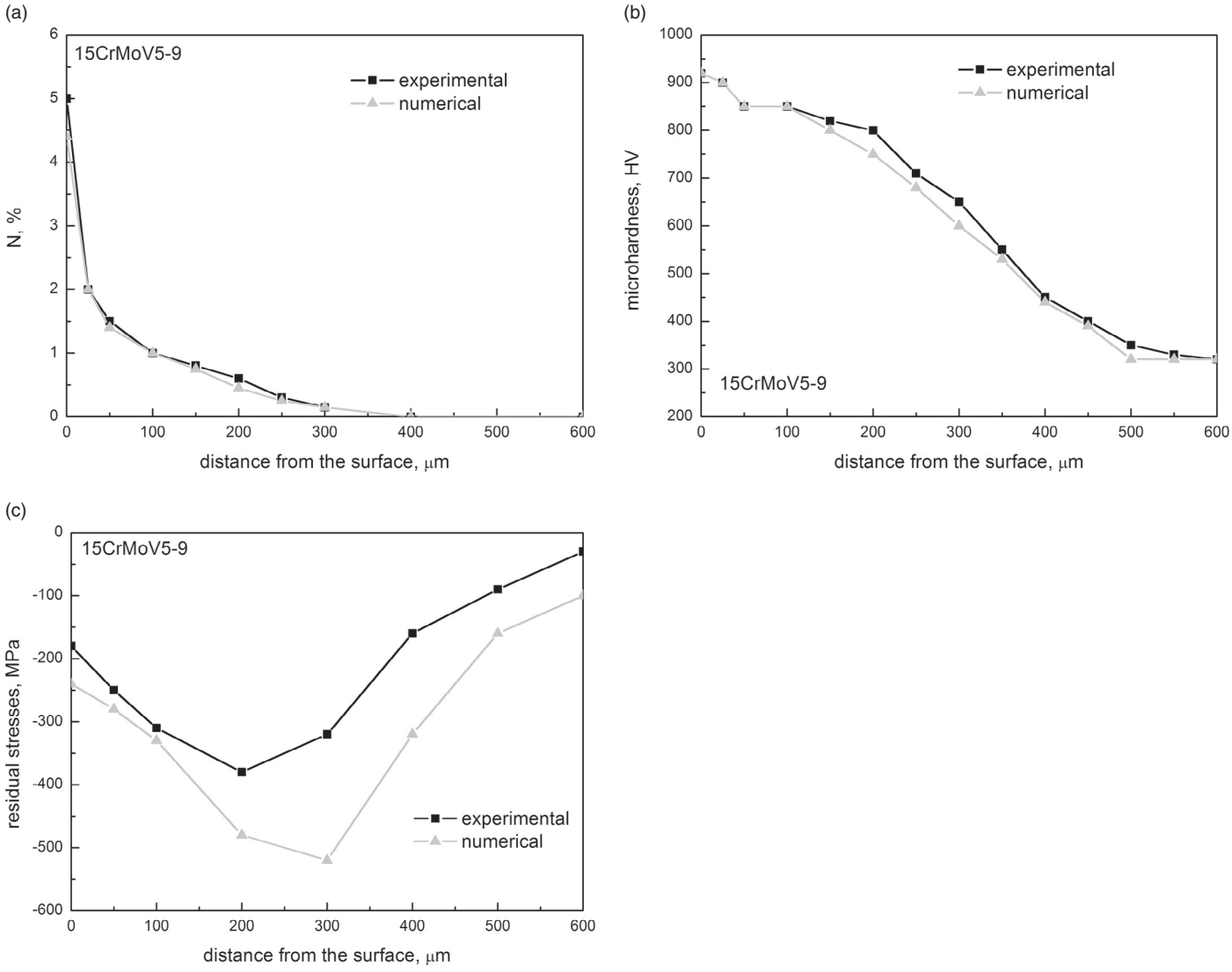

Fig. 17. Nitrogen concentration (a), microhardness (b) and residual stresses (c) as a function of the distance from the sample surface for the control design of 15CrMoV5-9 steel.

was obtained and the equations relating to microstructural and mechanical properties (nitrogen concentration, nitrides layers, microhardness and residual stresses) of different steels as a function of nitriding parameters were calculated. The calculations led to the definition of the independent coefficients solved by ANSYS through modeFRONTIER by matching in closed loops the solutions with the experimental data. In the validation phase, the correlation between experimental and numerical results (obtained by the previous described procedure) was analyzed for selected control design belonging to AISI1020, 15CrMoV5-9, 31CrMo12, 34CrAlNi7, 39MoAlCr15, AISI304, AISI420, M2, V2, 18HGT steel. At the end of the study, different designs optimized to achieve the maximization of surface and bulk hardness of the nitrided steel were identified.

Acknowledgments

The authors gratefully acknowledge ENGINSOFT S.p.A. for the technical support and the PUGLIA REGION for the foundlings provided to the project S.T.A.R.-EXD (Simulation Technology Aeronautic Research-Extended Data) in the program action "F.E.S.R. sul P.O. Regione Puglia 2007–2013, Asse I-Linea 1.1 – Azione1.1.2. Aiuti agli Investimenti in Ricerca per le PMI".

Appendix

$$
\begin{aligned}
\mathbf{N\_0} = {} & 1.1264495247462203 \\
& + ((((\cos(((1*(\mathrm{Mn}+\ln(\mathrm{Np})))/\cos((\exp(\mathrm{Cr})*(\mathrm{Ti}*\exp(\mathrm{Cr})))))) \\
& + (\cos((\cos((\mathrm{Ti}*\exp(t_N)))+((\exp(\mathrm{Ti})*\ln(T_N))+\ln(\mathrm{Np})))) \\
& + (\mathrm{Mn}+\ln(\mathrm{Np}))))*\cos((\exp((\ln(t_N)*((\mathrm{Mn}+\ln(\mathrm{Np})) \\
& *\sin(\mathrm{V}))))/t_N))) - \cos((((\cos((\mathrm{Ti}*\exp(\mathrm{Np})))t_N) \\
& + ((\ln(\mathrm{Np})/\cos((\mathbf{Ti}*\exp(\mathrm{Np}))))/\cos((\mathrm{Ti}*\mathrm{Ti}*\exp(\mathrm{Np})))))) \\
& *\cos(\exp(((\mathrm{Mn}+\mathrm{Mn})/\cos((1*\sin(\mathrm{Mn}))))))) \\
& + ((((((\mathrm{Ti}+\ln(\mathrm{Np}))*\cos((\ln(\mathrm{Np})/t_N))) \\
& *\cos((\cos((\mathrm{Ti}-\ln(T_N)))/t_N))) - \cos(((((\mathrm{C}+\exp(\mathrm{Ti})) \\
& *(\mathrm{Ti}+\ln(\mathrm{Np})))*\cos((\mathrm{Ti}*\exp(\mathrm{Np})))) \\
& *\cos(((\mathrm{Mn}+\ln(\mathrm{Np}))+\sin(\mathrm{V})))))*\cos((((\mathrm{Co}*\cos(\mathrm{Np}))*\cos(\mathrm{Np})) \\
& *\cos((\ln(\mathrm{Np})*\cos((\mathrm{Ti}*\mathrm{Si})))))) \\
& - \cos(\exp(((\mathbf{Mn}+\mathrm{Mn})/\cos((\mathrm{V}*\cos((\mathrm{Co}-\mathrm{Mn})))))))
\end{aligned}
$$

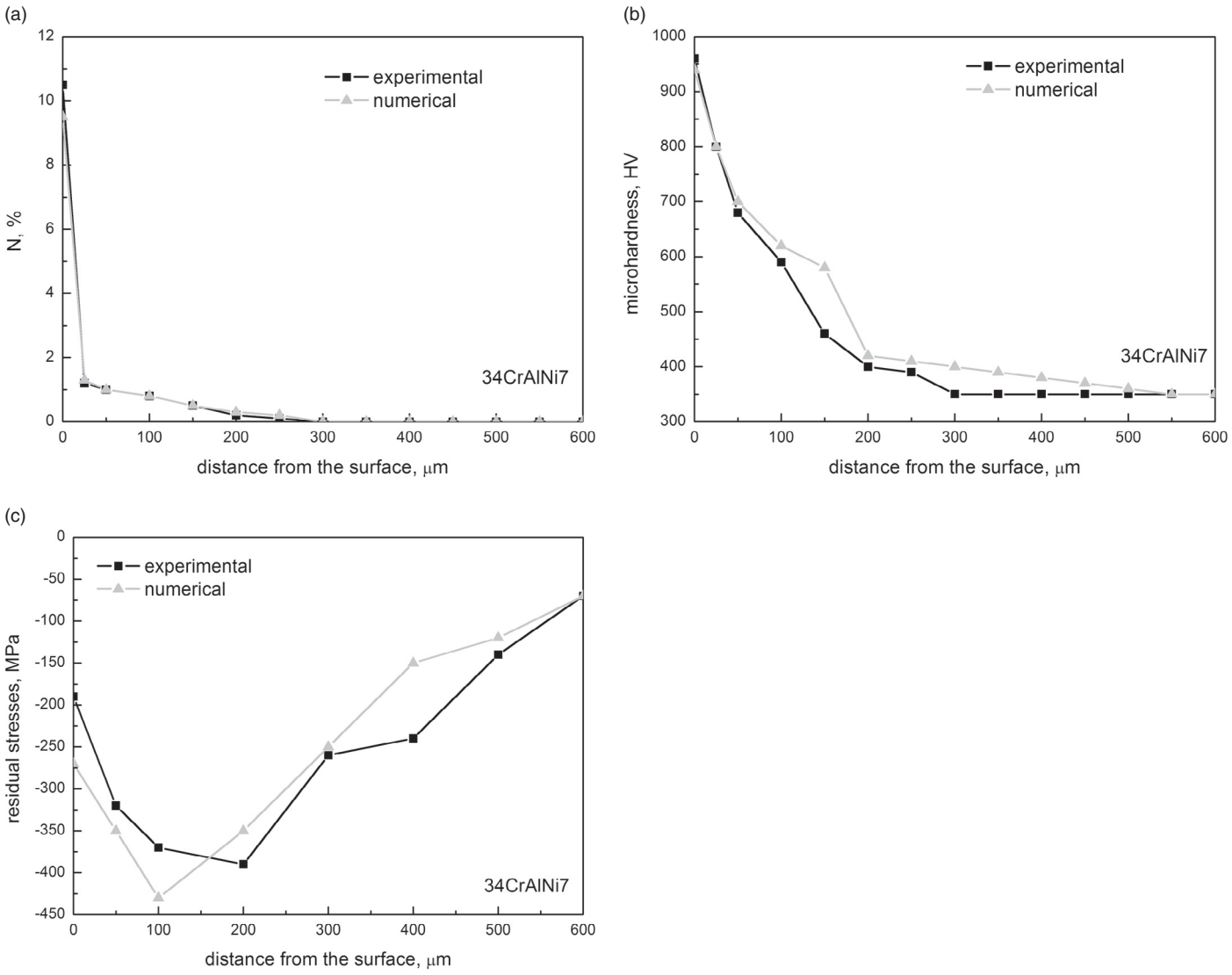

Fig. 18. Nitrogen concentration (a), microhardness (b) and residual stresses (c) as a function of the distance from the sample surface for the control design of 34CrAlNi7 steel.

Equation A1: Nitrogen concentration on the sample surface as a function of processing parameters and steel composition.

$$\begin{aligned}\mathbf{N\_200} = {} & -0.8191165912391943 \\ & + (\cos(\sin(\ln((T_N + ((((V * \exp(Mn)) * (\mathbf{W} * \cos(T_N))) \\ & - (Np/\cos(W))) * (((V + \exp(Mn)) + \cos(\exp(Mn))) \\ & - \sin(((V + T_N)/Fe))))))) \\ & + ((((V/Fe)/\exp(\sin(\sin(\cos(W))))))/\exp((Al \\ & * (((T_N + V) + T_N)/((\cos(T_N) + \cos(T_N)) \\ & - \ln((V + T_N)))))))/\sin(\ln(((T_N + ((V/\cos(T_H)) - \exp(Mn))) \\ & + ((((V/\cos(C)) + (\exp(Mn)/\cos(T_H))) + (\exp(\mathbf{Mn})/\cos(T_H))) \\ & + (\exp((\cos(T_N) + \cos(T_N))) * \cos(T_H))))))))\end{aligned}$$

Equation A2: Nitrogen concentration at a distance of 200 μm from the nitride surface as a function of processing parameters and steel composition.

$$\begin{aligned}\mathbf{HV\_0} = {} & 1202.6242028807285 + ((((((((((Cr/0.1) - (V/0.1)) \\ & - (Fe/(Mo + t_N))) - (((V/0.1) + 0.1) + (Ni + t_N))) \\ & - (Fe/((Al/0.1) + Np))) - ((Fe - ((Al - (T_N/10)) + 1))/(Cr \\ & + ((V/0.1) + 1)))) - (Fe/((Mo/(((Cr + 1)/(V + t_N))/(W + (W + t_N)))) \\ & + ((V/0.1) + 1)))) - ((Fe - (((Cr/0.1) - (Fe/((V/0.1) + 1))) \\ & + 1))/((V/((Cr + t_N)/((Fe + 10) + ((Cr + 1) - (V/0.1))))) \\ & + (((Al/(10/(t_N + t_N))) + Mn) + 1)))) - (((Fe - (((Cr/0.1) \\ & - (Fe/((V + t_N) + 1))) + Mo))/((V/((((Cr + 1) - (V/0.1)) \\ & - (Fe/(Cr + 1))) - ((10/(V + t_N)) + (W + t_N)))) + (((((Cr/0.1)/(W \\ & - Fe))/((Fe/t_N)/0.1)) + Mn) + 1)))/((V/(((Al(10/(W + Fe))) \\ & - (Fe/(S - (T_N/10)))) - ((Fe/(Cr + t_N)) \\ & + ((10/(Fe/t_N))/(C + (Cr + 1)))))) \\ & + ((((Al/(10/(0.1 + t_N)))/((10/(V + t_N))/(W + (Al + t_N)))) \\ & + (Mo/((10/(V + t_N))/(10/(Cr + 1))))) + 1)))) - (T_N/(Fe/((((Cr \\ & + 1) + 10) + V) + 10))))\end{aligned}$$

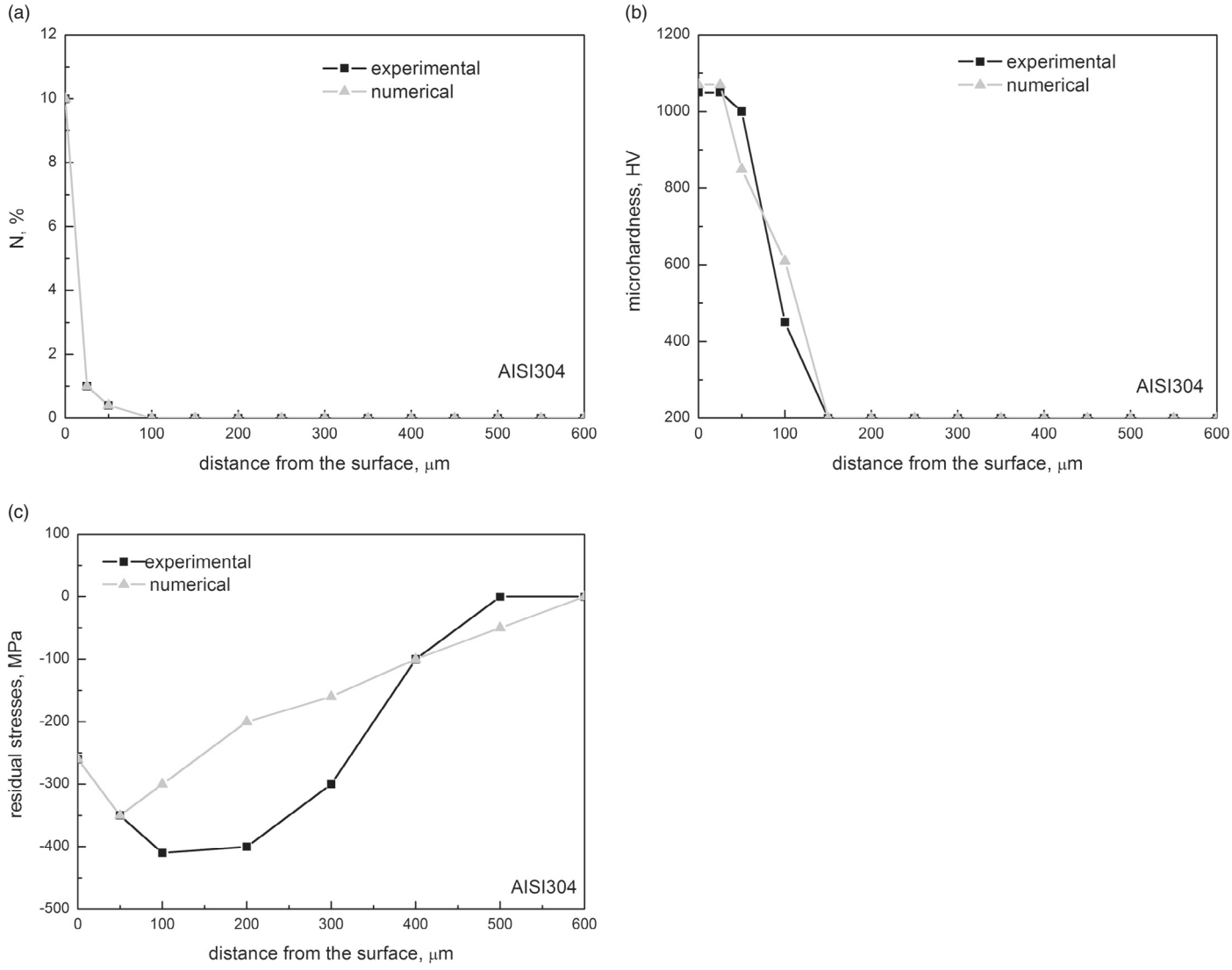

Fig. 19. Nitrogen concentration (a), microhardness (b) and residual stresses (c) as a function of the distance from the sample surface for the control design of AISI304 steel.

Equation A3: Hardness concentration on the sample surface as a function of processing parameters and steel composition.

$$\begin{aligned}\varepsilon_f = {} & -279.8784048207975 + ((((\cos((((\ln(T_N) - 0.1) \\ & + ((Mn - S)/(\ln(T_N) - \exp(C)))) + (((Ti - 0.1) - 0.1) \\ & + (\ln(T_N) + (\ln(T_N) + \ln(T_N))))))) * (\ln(((t_N + \exp(\exp(C))) \\ & + (((Mn - S) - \exp(1)) - Mo))) + (((\exp(C) - Si) \\ & - 0.1) - 0.1))) + (\cos(((\ln(T_N) - ((Mn - S)/(Mn - 0.1))) \\ & + (\ln((\ln(T_N) - (Mn - Ni))) + ((\ln(T_N) + Ni) + (\ln(T_N) \\ & + \ln(T_N)))))) + (((((\ln(T_N) - 0.1) + ((Mn - S)/(Mn - 0.1))) \\ & + ((\ln(T_N) - Si) + Al)) + (Al + (((Mn - 0.1) - 0.1) + (\ln(T_N) + \ln(T_N))))) \\ & + (\ln((t_N + \exp(\exp(C)))) + (\exp(C) - Si))))/0.1) - (((\exp(C) \\ & + ((\cos(T_N) + (\exp(C)/(((Mn - S)/(Mn - 0.1)) - \exp(C)))) \\ & + (\exp(C)/(((Mn - S)/(Mn - 0.1)) - \exp(C))))/(\ln((((\ln(T_N) \\ & - (Mn - S)) + \exp(1)) - (Mn - S))) + (((((Mn - S)/(Mn - 0.1)) \\ & - \exp(C)) - 0.1) + (\ln(T_N) + Ni)))) + (((((((Mn - 0.1) + (\ln(T_N) + \ln(T_N))) \\ & + (\ln(T_N) + \ln(T_N))) + (Al + ((\ln(T_N) - Si) + (\ln(T_N) + \ln(T_N))))) \\ & + (\ln((t_N + \exp(\ln(T_N)))) + ((\cos(T_N) + (\ln(T_N) + \ln(T_N))) \\ & - Si)))/((((\ln(T_N) - 0.1) - 0.1) - 0.1) \\ & - ((Mn - S)/(((Mn - S)/(Mn - 0.1)) \\ & - \exp(C))))) + Ni)))\end{aligned}$$

Equation A4: Thickness of the ε nitrides as a function of processing parameters and steel composition.

$$\begin{aligned}\gamma'_f = {} & 98.68824774543444 + (((Fe - (((((T_N * 0.1) - (\sin((V * 10)) * 10)) \\ & - ((\sin(\ln(T_N)) * 10) * 10)) - (\sin((((T_N * 0.1) - \ln(T_H))/\ln(T_H))) \\ & * (\ln(t_N) * 10))) - (Co - (((((T_N * 0.1) - (V - Np)) - (\ln(t_N) * 10)) \\ & - (\ln(t_N) - Np)) - (Al * ((\ln(t_N) * \ln(T_N)) - n(T_H))))))) \\ & + ((S - ((((((Mn/Np) + Fe) - ((Mn - Si) - (T_N * 0.1))) - ((T_N * 0.1) \\ & - 10)) - (\ln(T_H) * \ln(T_N))) - (Al * ((\ln(t_N) * (\ln(t_N) * 10)) \\ & - (((T_N * 0.1) - (Mn - Si)) - (\ln(t_N) * \ln(T_N)))))))/Np)) \\ & - (((((((T_N * 0.1) - ((Mn - Si) * 10)) - ((\sin(\ln(T_N)) * 10) * 10)) \\ & - ((((T_N * 0.1) - 10)/(S - 10))/(S - 10))) * \ln(10)) \\ & - ((\sin((((T_N * 0.1) - 10)/((\ln(T_H) * \ln(T_N)) - 10))) * (\ln(t_N) * 10)) \\ & - ((((((T_N * 0.1) - \ln(T_N)) - (\ln(t_N) * \ln(t_N))) - ((V * 10) + Fe)) \\ & - ((Mn - Si) * Cr)) - Fe))) - ((\sin((((T_N * 0.1) - 10)/((\ln(T_H) \\ & * \ln(T_N)) - 10))) * (\sin((((T_N * 0.1) - 10)/(S - 10))) * (\ln(t_N) * 10))) \\ & + ((Al/(((((S - Fe) - \ln(T_N)) - Np) - (((T_N * 0.1) - \ln(T_H)) \\ & - ((+ p\_Fe))) - Ni)) - (((((T_H * P) - (V * 10)) - 0.1) - (V + 10)) \\ & - (\sin((((T_N * 0.1) - 10)/(S - 10))) * (\ln(t_N) * 10)))))))\end{aligned}$$

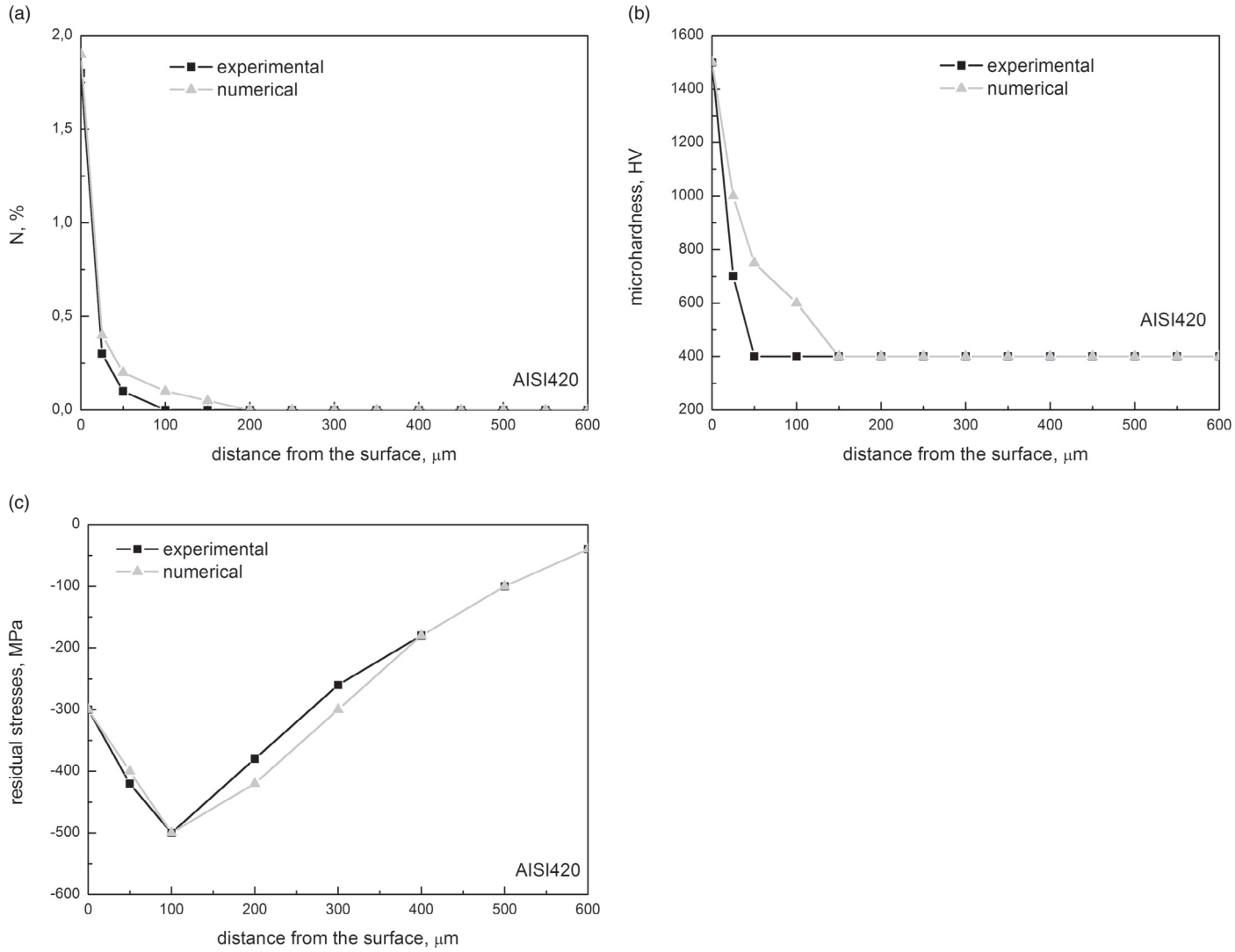

Fig. 20. Nitrogen concentration (a), microhardness (b) and residual stresses (c) as a function of the distance from the sample surface for the control design of AISI420 steel.

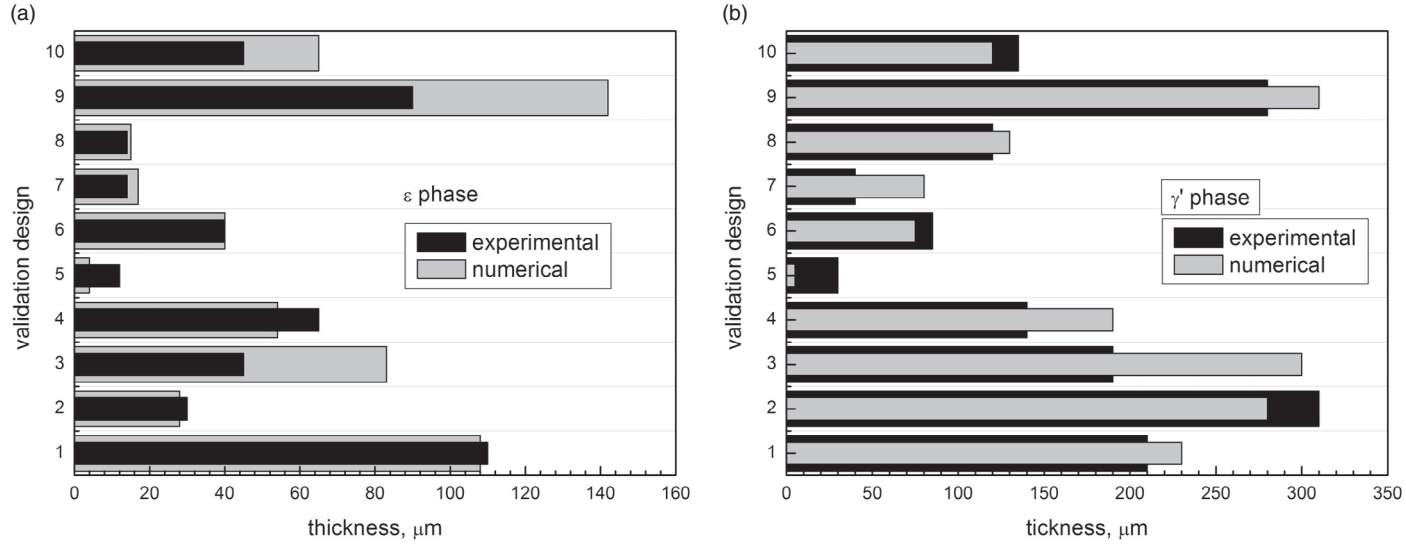

Fig. 21. Thickness comparison between numerical and experimental data for 10 control designs with regards to ε and γ' phases.

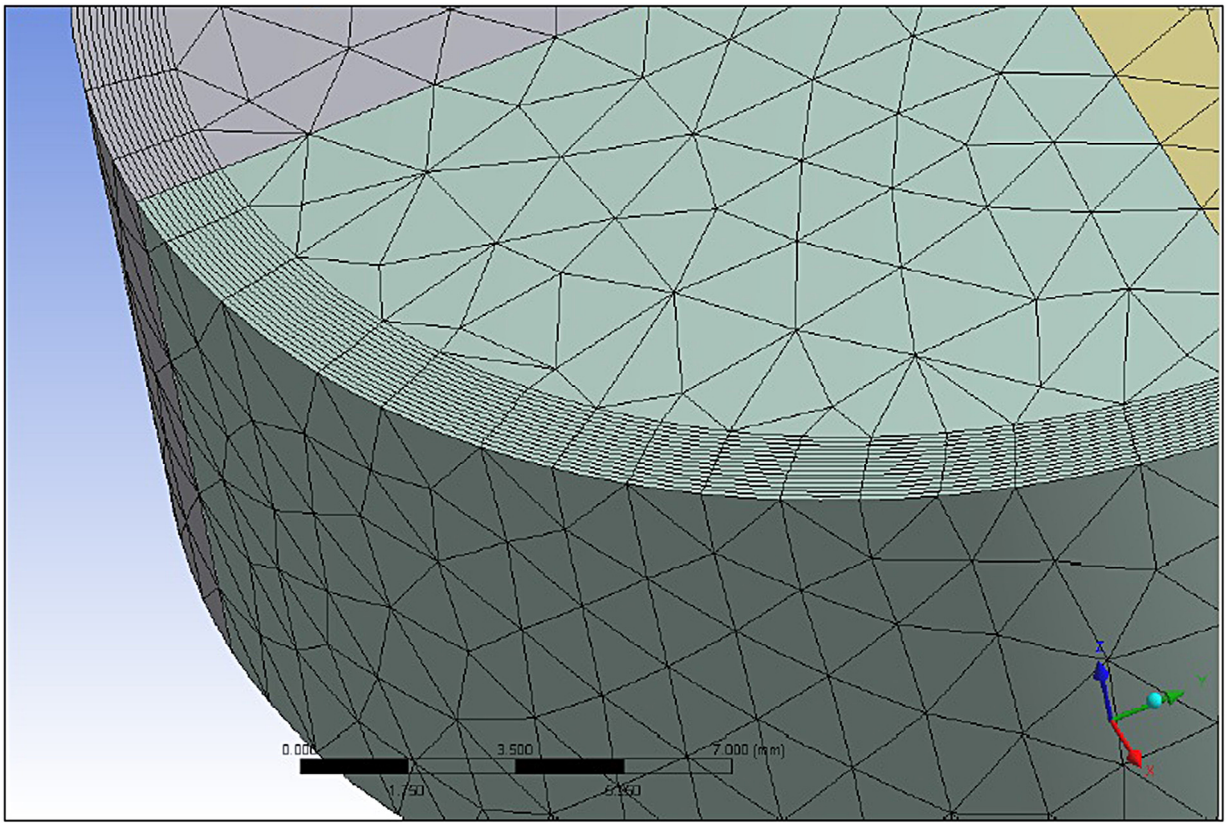

Fig. 22. Mesh geometry of the nitride samples.

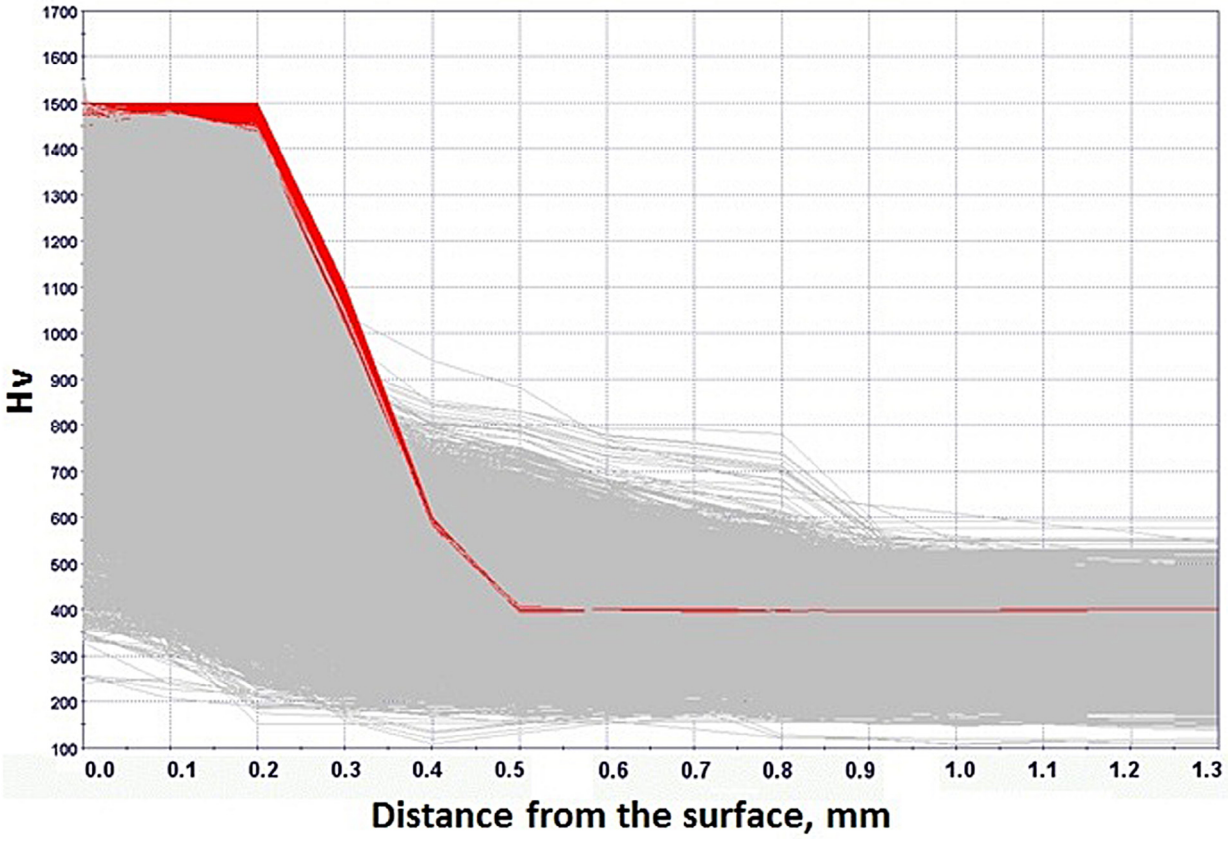

Fig. 23. Different hardness profiles as a function of the computational runs.

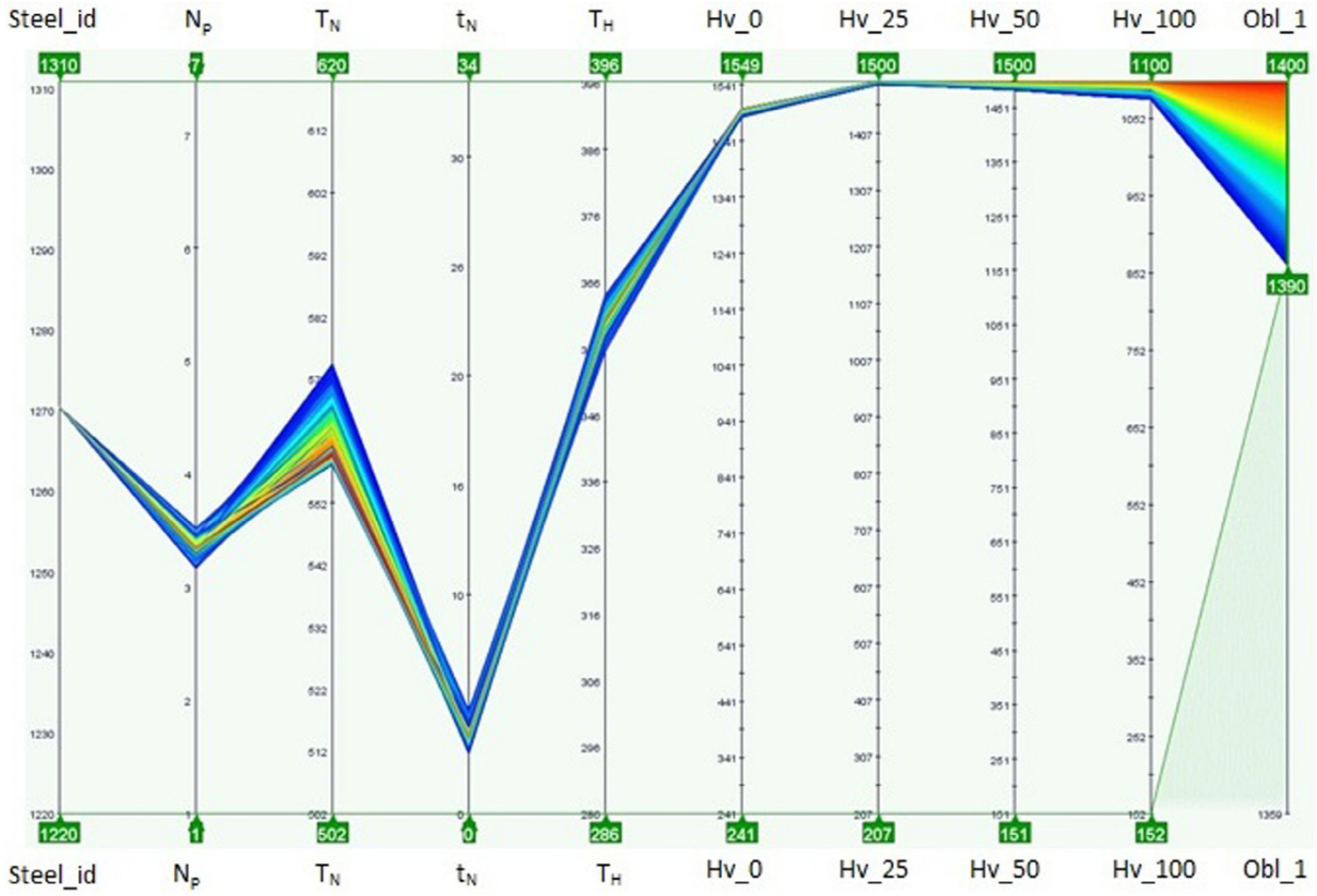

Fig. 24. Processing parameters chart for the optimized hardness profiles.

Equation A5: Thickness of the γ' nitrides as a function of processing parameters and steel composition.

Nomenclature

T_H	heat treatment temperature
N_p	nitrogen potential
T_N	nitriding temperature
t_N	nitriding time
N_xxx	nitrogen concentration at xxx μm from the surface
ε_s	distance from the surface of the starting point of ε phase
ε_f	distance from the surface of the ending point of ε phase
γ'_s	distance from the surface of the starting point of γ' phase
γ'_f	distance from the surface of the ending point of γ' phase
Hv_xxx	microhardness at xxx μm from the surface
σ_xxx	residual stresses at xxx μm from the surface

References

[1] P. Cavaliere, G. Zavarise, M. Perillo, Modeling of the carburizing and nitriding processes, Comput. Mater. Sci. 46 (1) (2009) 26–35.
[2] E.J. Mittemeijer, M.A.J. Somers, Thermodynamics, kinetics, and process control of nitriding, Surf. Eng. 13 (6) (1997) 483–497.
[3] B. Appolaire, M. Gouné, Linear stability analysis of a γ'-Fe4N nitride layer growing in pure iron, Comput. Mater. Sci. 38 (1) (2006) 126–135.
[4] M. Keddam, M.E. Djeghlal, L. Barrallier, E. Salhi, Computer simulation of nitrided layers growth for pure iron, Comput. Mater. Sci. 29 (1) (2004) 43–48.
[5] L. Torchane, P. Bilger, J. Dulcy, M. Gantois, Control of iron nitride layers growth kinetics in the binary Fe-N system, Metallurg. Mater. Trans. A 27A (1996) 1823–1834.
[6] V.I. Dimitrov, J.D. Haen, G. Knuyt, C. Quaeyhaegens, L.M. Stals, Modeling of nitride layer formation during plasma nitriding of iron, Comput. Mater. Sci. 15 (1) (1999) 22–34.
[7] S.S. Akhtar, A.F.M. Arif, B.S. Yilbas, Evaluation of gas nitriding process with in-process variation of nitriding potential for AISI H13 tool steel, Int. J. Adv. Manufact. Technol. 47 (5–8) (2010) 687–698.
[8] İ.B. Özdemir, N. Lippmann, Modeling and simulation of surface reactions and reactive flow of a nitriding process, Surf. Coat. Technol. 219 (2013) 151–162.
[9] D.Q. Peng, T.H. Kim, J.H. Chung, J.K. Park, Development of nitride-layer of AISI 304 austenitic stainless steel during high-temperature ammonia gas-nitriding, Appl. Surf. Sci. 256 (2010) 7522–7529.
[10] J.H. Kong, D.J. Lee, H.Y. On, S.J. Park, S.K. Kim, C.Y. Kang, et al., High temperature gas nitriding and tempering in 17Cr1Ni0.5C0.4V steel, Met. Mater. Int. 16 (2010) 857–863.
[11] H.W. Lee, J.H. Kong, D.J. Lee, H.Y. On, J.H. Sung, A study on high temperature gas nitriding and tempering heat treatment in 17Cr–1Ni–0.5C, Mater. Des. 30 (2009) 1691–1696.
[12] S.M. Hassani-Gangaraj, M. Guagliano, Microstructural evolution during nitriding, finite element simulation and experimental assessment, Appl. Surf. Sci. 271 (2013) 156–163.
[13] P. Kochmanski, J. Nowacki, Influence of initial heat treatment of 17-4 PH stainless steel on gas nitriding kinetics, Surf. Coat. Technol. 202 (2008) 4834–4838.
[14] S.J.B. Kurz, S.R. Meka, N. Schell, W. Ecker, J. Keckes, E.J. Mittemeijer, Residual stress and microstructure depth gradients in nitrided iron-based alloys revealed by dynamical cross-sectional transmission X-ray microdiffraction, Acta Mater. 87 (2015) 100–110.
[15] M. Keddam, B. Bouarour, R. Kouba, R. Chegroune, Growth kinetics of the compound layers: effect of the nitriding potential, Phys. Proced. 2 (2009) 1399–1403.
[16] S.S. Akhtar, A. Fazal, M. Arif, B.S. Yilbas, Influence of multiple nitriding on the case hardening of H13 tool steel: experimental and numerical investigation, Int. J. Adv. Manufact. Technol. 58 (2012) 57–70.

[17] A.F.M. Arif, S.S. Akhtar, B.S. Yilbas, Effect of process variables on gas nitriding of H13 tool steel with controlled nitriding potential, Int. J. Surf. Sci. Eng. 4 (2010) 396–415.
[18] H. Ju, L.X. Li, Q.B. Wang, J.P. Diao, Optimum design of the gas nitriding technological parameters of H13 steel, Gongneng Cailiao/J. Funct. Mat. 42 (2011) 405–407.
[19] M. Yang, C. Zimmerman, D. Donahue, R.D. Sisson Jr., Modeling the gas nitriding process of low alloy steels, J. Mater. Eng. Perform. 22 (2013) 1892–1898.
[20] M. Yang, R.D. Sisson Jr., Modeling the nitriding process of steels, Adv. Mater. Process. 170 (2012) 33–36.
[21] G.K. Williamson, W.H. Hall, X-ray line broadening from filed aluminium and wolfram, Acta Metallurg. 1 (1) (1953) 22–31.
[22] P. Cavaliere, A. Perrone, A. Silvello, J. Manufact. Process. 17 (2015) 9–27.